Facultative chemosynthesis in a deep-sea anemone from hydrothermal vents in the Pescadero Basin, Gulf of California

Authors: Shana K Goffredi[1*], Cambrie Motooka[1], David A. Fike[2], Luciana C Gusmão[3], Ekin Tilic[4], Greg W Rouse[5], Estefanía Rodríguez[3]

[1] Occidental College, LA USA,
[2] Washington University, St Louis, MO USA,
[3] American Museum of Natural History, NY USA,
[4] University of Bonn, Germany,
[5] Scripps Institution of Oceanography, CA USA

*To whom correspondence may be addressed. Email: sgoffredi@oxy.edu

Keywords (3-10): Actiniaria**,** chemoautotrophic, SUP05, Gulf of California, Pescadero Basin, sulfide-oxidizing, symbiosis, chemosynthetic, *Ostiactis*

Abstract:

Background

Numerous deep-sea invertebrates have formed symbiotic associations with internal chemosynthetic bacteria in order to harness inorganic energy sources typically unavailable to most animals. Despite success in nearly all marine habitats and their well-known associations with photosynthetic symbionts, Cnidaria remain one of the only phyla without a clear dependence on hydrothermal vents and reliance on chemosynthetic bacterial symbionts specifically.

Results

A new chemosynthetic symbiosis between the sea anemone *Ostiactis pearseae* (Daly & Gusmão, 2007) and intracellular bacteria was discovered at ~3700 m deep hydrothermal vents in the southern Pescadero Basin, Gulf of California. Unlike most sea anemones observed from chemically-reduced habitats, this species was observed in and amongst vigorously venting fluids, side-by-side with the chemosynthetic tubeworm *Oasisia* aff. *alvinae*. Individuals of *O. pearseae* displayed carbon, nitrogen, and sulfur tissue isotope values (average $\delta^{13}C$ -29.1‰, $\delta^{15}N$ 1.6‰, and $\delta^{34}S$ -1.1‰) suggestive of a distinct nutritional strategy from conventional Actiniaria suspension feeding or prey capture. Molecular and microscopic evidence confirmed the presence of intracellular SUP05-related bacteria housed in the tentacle epidermis of *O. pearseae* specimens collected from 5 hydrothermally-active structures within two vent fields ~2 km apart. SUP05 bacteria dominated the *O. pearseae* bacterial community (64-96% of the total bacterial community based on 16S rRNA sequencing), but were not recovered from other nearby anemones, and were generally rare in the surrounding water (< 7% of the total community). Further, the specific *Ostiactis*-associated SUP05 phylotypes were not detected in the environment, indicating a specific association. Two unusual candidate bacterial phyla (the OD1 and BD1-5 groups) also appeared to associate exclusively with *O. pearseae* and may play a role in symbiont sulfur cycling.

Conclusion

Ostiactis pearseae represents the first member of Cnidaria described to date to have a physical and nutritional alliance with chemosynthetic bacteria. The facultative nature of this symbiosis is consistent with the dynamic relationships formed by both the SUP05 bacterial group and Anthozoa. The advantages gained by appropriating metabolic and structural resources from each other presumably contribute to their striking abundance in the Pescadero Basin, at the deepest known hydrothermal vents in the Pacific Ocean.

Background

Numerous deep-sea annelids, molluscs, and other invertebrates have forged relationships with bacteria in order to harness inorganic sources of energy that are typically unavailable to most animals. Microbial chemosynthesis generates energy through the oxidation of sulfide, as an example, used to fuel the production of organic carbon, which can be shared with a receptive animal host. To date, members of at least six major animal clades, including most recently *Trichoplax* (Placozoa), have formed symbiotic associations with internal chemosynthetic bacteria (Dubilier 2008; Gruber-Vodicka et al. 2019). Interestingly, Cnidaria, although well-known to host photosynthetic symbionts, remains one of the last prominent animal clades without a documented metabolic dependence on chemosynthetic bacterial symbionts for survival in hydrothermal vents.

Anthozoa, which includes sea anemones and corals, is among the most successful and diverse group of Cnidaria, found in all marine habitats at most depths and latitudes (Daly et al. 2008). Their worldwide ecological success may best be attributed to an ability to form symbiotic relationships with other organisms, including microbial eukaryotes (e.g. the dinoflagellate *Symbiodinium*; LaJeunesse et al. 2018), as in the case of shallow-water tropical species. Anthozoa such as sea anemones, octocorals and zoanthids are also found at deep-sea reducing environments, such as hydrothermal vents, seeps, and whalefalls (Daly and Gusmão 2007; Zelnio et al 2009; Rodríguez et al. 2012; Breedy et al. 2019), however they have been historically understudied, and most remain undescribed. It would be reasonable, and perhaps even expected, for some of these deep-sea Anthozoa to also host microbial symbionts. In fact, a recent study demonstrated an affiliation between sulfide-oxidizing bacteria and certain species of Anthozoa found near deep-sea methane seeps, however the specific mode and importance of this relationship is not yet known (Vohsen et al. 2020).

The recently discovered Pescadero Basin vent field at 3700 m depth in the southern Gulf of California differs markedly from nearby vent localities (e.g. Guaymas Basin and 21°N East Pacific Rise) in physical, chemical, and biological attributes (Caress et al. 2015; Goffredi et al. 2017; Paduan et al. 2018). In particular, the vents in the Pescadero Basin are uniquely composed of hydrothermal calcite, with venting fluids that contain high levels of aromatic hydrocarbons, hydrogen, methane and hydrogen sulfide at a pH of ~6.5 (Goffredi et al. 2017). The Pescadero Basin vents are also highly unusual in faunal composition with many new species and numerous others that do not occupy nearby regional vents (e.g. Alarcon Rise vents; Rouse et al. 2016; Goffredi et al. 2017; Hatch et al. 2020). Included in this group of unusual fauna was a very abundant white sea anemone (up to 68 individuals m^{-2} in some areas) that occurred in and amongst the siboglinid tubeworm *Oasisia* aff. *alvinae*, often very near to actively venting fluids (Fig.

1; Supplemental Video; Goffredi et al. 2017).

Previously, several unidentified Pescadero Basin Actiniaria (sea anemones) were reported to be quite depleted in tissue $\delta^{13}C$ values (-33 to -38‰; Goffredi et al. 2017; Salcedo et al. 2019). This evidence, along with their unusual life position and abundance in zones of active fluid venting, hinted at their possible nutritional reliance on chemoautotrophic carbon production, as opposed to traditional suspension feeding or prey capture via cnidae, however, the specific details were not explored further. Here, by combining microbial community profiling, ultrastructural analysis via microscopy, and stable isotope measurements, we document the first species of chemosynthetic sea anemone at vents deep in the Gulf of California, identified as *Ostiactis pearseae* (previously known only from whalefalls; Daly and Gusmão 2007). This extensive new population of *O. pearseae* appears to rely on nutritional supplementation of carbon, nitrogen, and sulfur by intracellular bacteria within the SUP05 clade, housed in their epidermis.

Results

Actiniaria of various morphotypes were observed to be one of only a handful of dominant animal species in both the Pescadero Basin Auka vent field (Goffredi et al. 2017; Paduan et al. 2018) and the newly discovered JaichMaa 'ja'ag vent field, both within ~2 km of each other in the Gulf of California (Fig. 1). A conspicuous white actiniarian species visually represented a significant fraction of the animal community and was collected from 5 vent edifices in zones of active venting, very near to the obligate vent tubeworm, *Oasisia* aff. *alvinae* (Fig. 1). Several other sea anemones (by morphotype) were observed and collected near these same sites, usually in areas of less active fluid flow (Table 1). The white actiniarian morphotype was identified as *Ostiactis pearseae* (Daly and Gusmão, 2007), based on anatomical, cnidae and DNA sequencing of preserved polyps. The Pescadero Basin populations of *O. pearseae* showed slight differences in morphology and cnidae to the description of specimens from the type locality and, thus, an amendment to the species diagnosis is provided.

Class Anthozoa Ehrenberg, 1834
Subclass Hexacorallia Haeckel, 1896
Order Actiniaria Hertwig, 1882
Suborder Enthemonae Rodríguez and Daly, 2014 in Rodríguez et al. 2014
Superfamily Metridioidea Carlgren, 1893
Family Ostiactinidae Rodríguez et al. 2012
Genus *Ostiactis* Rodríguez et al. 2012
Ostiactis pearseae (Daly & Gusmão, 2007)
(Figures 2-3, Table 2; Table S2)

Diagnosis: (amended after Daly and Gusmão, 2007 and Rodríguez et al. 2012, modifications in italics). Ostiactinidae with basilar muscles and mesogleal marginal sphincter. Body with well-developed base. Column not clearly divisible into scapus and scapulus; scapus without cuticle, *maybe* with scattered demarcated suckers distally; column without cinclides *or with a distal row of round papillae with inconspicuous cinclides*. Tentacles regularly arranged, not thickened on the aboral side. Six pairs of perfect and fertile mesenteries, hexamerously arranged, not divisible into macro- and micro-cnemes. *Same number of mesenteries proximally and distally*. Retractor muscles weak but *restricted*. No acontia. *Some populations with chemosynthetic bacteria in tentacles*. Cnidom: Robust spirocysts, basitrichs, holotrichs, and *p-mastigophores A and B1*. *Ostiactis pearseae* had been previously collected only in deep-sea waters (2800 m depth) of the Eastern Pacific, at a whalefall habitat in Monterey Bay (Daly & Gusmão 2007). Newly collected specimens are from deep-sea waters (3655-3692 m depth) associated with Southern Pescadero Basin hydrothermal vents (Diane's vent) in the Gulf of California (Pacific Ocean).

Intrapopulation variability in morphology was observed in the Pescadero Basin *Ostiactis pearseae* specimens (Fig. 2). Differences were observed mainly in the abundance and categories of cnidae among specimens (particularly holotrichs in the column), but also in the presence of a distal row of papillae (with only basitrichs) associated with inconspicuous cinclides in two specimens (SO197-S2 and SO200-R2; Fig. 2). Because of the small size of the papillae, the relatively small sizes and state of contraction and preservation condition of the specimens, it is not definitive that this row of distal papillae is only present in these two individuals. Nevertheless, the rest of the morphological and molecular characters, as well as the cnidae data, from the specimens with distal papillae agree with those of the other specimens studied, suggesting that differences should be treated as intrapopulation variation. Morphologically, specimens of *O. pearseae* from the Pescadero Basin possess ~70 tentacles, compared to specimens of similar sizes from the type locality, described as having ~100 tentacles (Daly & Gusmão 2007), with some having poorly demarked suckers in the column (which were not observed in Pescadero Basin specimens). Additionally, the first and second cycles of mesenteries are fertile in the type specimens, with males observed brooding larvae internally in the tentacles (Daly & Gusmão 2007). Although the fertility of the first cycle could not be confirmed for the Pescadero Basin specimens, the second and third cycles were confirmed to be fertile, but no brooding individuals were identified. The previous implementation of a different cnidae terminology suggests conspicuous differences in cnidae types and sizes between specimens at the Monterey Canyon whalefall and Pescadero Basin (Table 2), but a new more precise combined terminology used here allows for distinction within *p*-mastigophore capsules (i.e. *p*-mastigophores A and *p*-mastigophores B1). The types and size ranges of the original description and the newly collected specimens of *O. pearseae*

mostly agree (with only slight variability in some size ranges), with the only distinct difference being the presence of *p*-mastigophores B1 capsules in the tentacles of the whalefall specimens, and not the Pescadero Basin specimens (Table 2).

All molecular phylogenetic analyses, based on the concatenated mitochondrial 12S rDNA, 16S rDNA, COIII genes and partial nuclear 18S rDNA gene were congruent and revealed a well-supported clade comprised of specimens of *Ostiactis pearseae* from Pescadero Basin and the type locality of Monterey Canyon (Fig. 3). DNA sequences from the Pescadero Basin specimens were identical to the Monterey Canyon population for 3 of the genes analyzed, and only differed from the type locality by 1-bp for the 16S rDNA gene. *Ostiactis* was recovered within Metridioidea, as sister to a weakly supported clade formed by deep-sea Actiniaria and those associated with chemosynthetic environments (e.g. clades Deepsina + Chemosynthina, as part of the family Kadosactinidae, sensu Rodríguez et al. 2012), a relationship consistent over different studies (e.g. Rodríguez et al. 2012, 2014; Grajales and Rodríguez 2016; Gusmão et al. 2019). Most representatives from these two clades are characterized by the loss of acontia (filament-like structures packed with nematocysts), the presence of which is a mayor synapomorphy for Metridioidea. The other actiniarian morphotype included here, identified as Kadosactinidae 'sp.B', was recovered (only mitochondrial sequence data available for this specimen) sister to *Alvinactis chessi*, a sea anemone inhabiting hydrothermal vents in the southwestern Pacific (Fig. 3; Zelnio et al. 2009).

Isotope signatures of **Ostiactis pearseae** *from the Pescadero Basin*

Tissue stable $\delta^{13}C$, $\delta^{15}N$ and $\delta^{34}S$ isotope values were significantly different for *Ostiactis pearseae* than other anthozoans at the Pescadero Basin vent fields (ex. zoanthids; Fig. 4A). For example, *O. pearseae* had $\delta^{13}C$ tissue values of -29.1 ± 4.6‰ (n = 9), while the others measured -20.6 ± 2.7‰ (n = 10; ± 1 SD; ANOVA p = 0.0001; Fig. 4A). Similarly, *O. pearseae* had much more negative $\delta^{15}N$ tissue values of 1.6 ± 1.7‰, whereas the others measured 10.6 ± 6.3‰, a difference of ~9‰ (± 1 SD; ANOVA p = 0.0006; Fig. 4A). Low $\delta^{15}N$ values were also observed in nearly all individuals of the Kadosactinidae 'sp.B' (~0.5-2.8; Fig. 4A) collected at the same locality. By comparison, *O. pearseae* was significantly more negative in both tissue $\delta^{13}C$ and $\delta^{15}N$ than four methane seep-associated octocoral species recently reported on by Vohsen et al. 2020 (ANOVA p = 0.0013 and p < 0.00001, respectively, n = 21; Fig. 4A). Finally, *O. pearseae* had significantly lower $\delta^{34}S$ tissue values of -1.1 ± 6.4‰ (n = 7), compared to other Pescadero Basin sea anemones (8.9 ± 5.2‰; n = 6; ANOVA p = 0.008), with comparable total tissue sulfur ~ 0.9-1.9% by weight (Fig. 4B).

Bacterial community analysis of Ostiactis pearseae *from the Pescadero Basin*

In *Ostiactis pearseae,* the tentacles are smooth, tapering and relatively long when extended, with features similar to most other anemones, including cnidocytes (or cnidoblasts), cnidocysts and glandular cells, all common cellular components sea anemones tentacles (Fautin & Mariscal 1991). Daly & Gusmão (2007) did not detect the presence of bacteria in the type specimens of *O. pearseae* from Monterey Canyon, however, the unusual isotope signatures of the Pescadero Basin specimens (Goffredi et al. 2017; Salcedo et al. 2019) prompted a more careful examination of this possibility. Indeed, bacterial community analysis via 16S rRNA Illumina barcoding revealed a dominance of the gammaproteobacteria SUP05 clade (64-96% of the bacterial community), comprising 6 putative sulfide-oxidizing bacterial OTUs (= phylotypes, clustered at 99% similarity) associated with the tentacles of Pescadero Basin *O. pearseae* (n = 8 specimens; Fig. 5, Table S1). This was in contrast to the sulfide-oxidizing gammaprotebacteria recovered from the nearby obligate vent tubeworms *Riftia pachyptila* and *Oasisia* aff. *alvinae* (100% identical to Candidatus *Endoriftia persephone*; Fig. 5A; Robidart et al. 2008). The SUP05 clade was not detected in association with 6 other individual sea anemones (determined by morphotype or molecular sequencing) and the specific *Ostiactis*-associated SUP05 phylotypes were not detected in surrounding water samples (n = 3; Fig. 5). Three SUP05 OTUs comprised 5-7% of the bacterial community in the surrounding water column (Fig. 5A), but were distinct, based on the 250-bp 16S rRNA Illumina barcode sequences (Fig. S1 inset).

NMDS ordination revealed the total bacterial community of *Ostiactis pearseae* to be strongly differentiated from those associated with zoanthid specimens (Analysis of Similarity (ANOSIM) R = 0.99, p = 0.002), the other unidentified sea anemone Kadosactinidae 'spB' (ANOSIM R = 0.87, p = 0.022), the water column samples (ANOSIM R = 1.00, p = 0.006), and the neighboring obligate vent tubeworms *Riftia pachyptila* and *Oasisia* aff. *alvinae* (ANOSIM R = 1.00, p = 0.001; Fig. 5C). Bacterial community analysis revealed limited diversity within the tentacles of *O. pearseae* from the 5 different Pescadero Basin vent sites (Fig. 5A; Table S1). Other bacteria uniquely recovered from *O. pearseae* tentacles included the BD1-5 group (a.k.a. Gracilibacteria; present in 5/8 *O. pearseae* specimens at 3-27%) and the OD1 group (a.k.a. Parcubacteria; present in 5/8 *O. pearseae* specimens at 1-16%; Fig. 5A). Additional bacterial groups present in non-*Ostiactis* sea anemones included Enterobacteriacea and Mollicutes (the latter 89% similar to one recovered from an ascidian; Fig. 5A; EF137402; Tait et al. 2007). Microbial groups that were more common in all 3 water samples included the Methylococcales marine group 2 (MMG-2), Rhodobiacea, and Thaumarcheota (Fig. 5A).

To further characterize the SUP05 in association with *Ostiactis pearseae*, a longer region of the 16S rRNA gene was amplified via direct PCR and sequenced. A 1334-bp long 16S rRNA sequence, only 1-bp different from barcode OTU21762, was 96.5% similar to a free-living bacterium from a mud volcano in the Eastern Mediterranean Sea (AY592908; Heijs et al. 2005) and 95% similar to the thiotrophic symbiont of *Bathymodiolus* aff. *brevior* from Central Indian Ridge vents (DQ077891; McKiness and Cavanaugh 2005; Fig. S1). There are no *Bathymodiolus* mussels at the Pescadero Basin vents, and the SUP05-related sequences recovered from *O. pearseae* are distinct from those recovered from *Bathymodiolus* from Costa Rica seeps, some of the closest known mussel populations (only ~96% similar for 250bp barcode sequence; Fig. S1 inset; Levin et al. 2012; McCowin et al. in press).

Several genes were additionally amplified and directly sequenced in order to inform the possible metabolic capabilities of the SUP05-related bacteria in *O. pearseae.* The *napA* gene, encoding a catalytic subunit of the periplasmic nitrate reductase alpha subunit (E.C. 1.7.99.4; Flanagan et al. 1999), amplified from *O. pearseae* tentacles, was most closely related (82-85% similarity based on amino acid translation; 77% based on nucleotides), to the *napA* gene from known SUP05 bacteria, including those from an estuary (ACX30474; Walsh et al. 2009) and the endosymbiont from *Bathymodiolus* mussel gill tissues (SMN16186). The *aprA* gene, encoding the adenosine phosphosulfate (or APS) reductase alpha subunit (E.C.1.8.99.2), recovered from *O. pearseae,* was most closely related to the *aprA* gene from the bacterial symbiont of a nematode from (96% similarity based on amino acid translation, ACF93728) and the endosymbiont of *Bathymodiolus septemdierum* (81% similarity based on nucleotide sequence, AP013042; Fujiwara et al. 2000).

Abundant SUP05 bacteria were observed embedded within the tentacle epidermis of *Ostiactis pearseae* (Fig. 6). Fluorescent *in situ* signal amplification via hybridization chain reaction-FISH (HCR-FISH) was necessary to overcome the very highly autofluorescent cnidae produced by the epidermis (Fig. 6G). HCR-FISH and TEM microscopy revealed intracellular cocci-shaped cells (~0.5 μm diameter), positioned just above or immediately adjacent to cnidae capsules and nuclei (Fig. 6G,I-J). These cells were definitively identified as members of the SUP05 group, given the consistent overlap between cells hybridized using a general bacterial probe set (Eub338-I-III) and a probe designed specifically to target the *O. pearseae* SUP05 (Fig. S2). Although poor tissue fixation somewhat compromised high-resolution electron microscopy (ex. many host cells were visibly ruptured with jumbled mitochondria), TEM provided additional evidence of symbiont integration within *O. pearseae*. Bacteria within the tentacles appeared concentrated in the periphery of cells within the mono-layered epidermis (Fig. 6I). Additionally, glands with large electron dense vesicles were observed occasionally

between the very elongated bacteria-containing cells (Fig. 6G) and a layer of mucous was observed overlying the epidermis in some instances. Bacteria on the tentacle surface occasionally appeared to be in clathrin-coated pits in various stages of endocytosis (Fig. 6L). For both microscopy methods, bacteria were not observed in either the gastrodermis or mesoglea of *O. pearseae* (Fig. 6G).

Discussion

A conspicuous actiniarian species, identified as *Ostiactis pearseae* (Daly & Gusmão, 2007), was dominant at two neighboring hydrothermal vent fields in the Pescadero Basin, Gulf of California. Unlike most vent anemones, which are almost always observed in the vent periphery, this species was found very near to vigorous venting fluids on and among the obligate vent tubeworms *Oasisia* aff. *alvinae* and *Riftia pachyptila* (Fig. 1), known to rely exclusively on sulfide-based chemosynthesis for energy (Fisher et al. 1989; Van Dover & Fry 1989). *Ostiactis pearseae*, formerly named *Anthosactis pearseae* (see Rodríguez et al. 2012), had been originally described as the first and only endemic Actiniaria from a whalefall community (Daly & Gusmão 2007), however, this discovery at hydrothermal vents makes them one of the only sea anemones described from multiple chemosynthetic environments (Zelnio et al. 2009; Rodríguez et al. 2012). The assumption, until now, was that most sea anemones at hydrothermal vents and methane seeps acquire nutrients via suspension feeding. Daly & Gusmão (2007) previously found no evidence that *Ostiactis pearseae* harbored chemosynthetic bacteria and accepted that they fed upon dissolved and particulate organic matter and plankton. However, the significantly negative $\delta^{13}C$ and $\delta^{15}N$ tissue isotopic values of *O. pearseae* (at the time labeled as an unidentified species in Goffredi et al. 2017 and Salcedo et al. 2019), suggested an entirely different strategy dependent upon bacteria chemosynthesis.

Indeed, distinct bacterial phylotypes related to the SUP05-group were associated with *Ostiactis pearseae*, compared to other nearby sea anemones and water column bacterial communities. This association was pervasive and dominant, in that SUP05 bacteria were found in all 8 *O. pearseae* specimens analyzed, comprising up to 96% of the recovered microbial 16S rRNA genes. Sulfur-oxidizing bacteria within the SUP05 clade, named after discovery in the Suiyo seamount plume (Sunamura et al. 2004), have been found worldwide in marine oxygen-deficient marine environments, deep-sea hydrothermal systems, and productive upwelling regions (Labrenz et al. 2007; Ulloa et al. 2012; Glaubitz et al. 2013). They exist both as free-living cells (Walsh et al. 2009) and in association with animal hosts (ex. *Bathymodiolus* mussels and some sponges; Petersen et al. 2012), where they participate centrally in the provisioning of fixed carbon to the animal.

Intracellular SUP05 were observed exclusively in the epidermis of *Ostiactis pearseae*, which was unexpected given that most Cnidaria house symbionts, mainly photosynthetic, in the gastrodermis (McAuley 1985; Marlow & Martindale 2007; Mellas et al. 2014). Epidermal bacteriocyte-like structures containing *Vibrio* have been observed in *Exaiptasia pallida* (Palincsar et al. 1989) and bacterial 'aggregates' containing *Endozoicimonas* have been observed in epidermal 'caverns' in the sea anemone *Metridium senile* (Schuett et al. 2007). In both cases, however, the epidermal bacteria are pathogens commonly associated with animals (Preheim et al. 2011; Neave et al. 2016). Vohsen et al. (2020) reported SUP05, and other bacteria, associated with whole octocoral specimens, including mucous, however the specific location of these bacteria was not determined. Interestingly, bacteria on the tentacle surface of *O. pearseae* appeared to be in clathrin-coated pits in various stages of endocytosis. Further examination of this receptor-mediated process is necessary to establish whether bacteria are actively transported inside of host cells and if so, what influences the recognition and selectivity of this process.

Hosting sulfide-oxidizing SUP05 in the outer epidermis may allow *Ostiactis pearseae* to avoid sulfide toxicity or the costly evolution of unique biochemistry to take up and transport sulfide (Goffredi et al. 1997). Additionally, the epidermis in Anthozoa can function in nutrition (Fautin & Mariscal 1991), even more so than the gastrodermis, through direct uptake of dissolved organic compounds (Schlichter 1975, 1980), thus the positioning of nutritional bacteria in the epidermis may increase effective exchange of small molecules. Like other SUP05 cells, those associated with the tentacles of *O. pearseae* were small (~500 nm in diameter; Shah et al. 2019). Presumably these symbionts require both oxygen and sulfide near simultaneously, for example "*Candidatus* Thioglobus autotrophicus", a member of the SUP05 group, has an aerobic phenotype, and uses sulfide while respiring oxygen (Marshall and Morris 2013; Shah et al. 2019). In this regard, it would be reasonable to house bacteria as close to the tissue surface as possible in order to accommodate gas exchange and meet symbiont metabolic demands.

The assumption that the SUP05 group may perform a nutritional role for the Pescadero Basin *Ostiactis pearseae* is evidenced by the comparatively light tissue $\delta^{13}C$ values (average -29.1‰). The contribution of chemosynthesis-derived carbon to *O. pearseae* biomass appears to exceed that reported for deep-sea anthozoan species from the Gulf of Mexico (ex. *Swiftia* and *Acanthogorgia*; Vohsen et al. 2020). The facultative nature of the SUP05-Anthozoa symbioses proposed by Vohsen et al. 2020 is also suggested for *O. pearseae* given the large range in negative $\delta^{13}C$ values observed. Like all sea anemones (even those with photosynthetic symbionts), *O. pearseae* retains an arsenal of nematocysts by which to capture prey, thus the SUP05 symbionts likely provide only a portion of their diet.

The SUP05 clade is not only involved in mediating dark carbon fixation, but also the cycling of nitrogen, whether by denitrification, as has been shown in free-living SUP05 populations (Walsh et al. 2009; Glaubitz et al. 2013) or assimilatory nitrate reduction, as in the case of symbiotic SUP05 (Ikuta et al. 2016; Vohsen et al. 2020). Significant contribution to tissue nitrogen by microbial nitrate utilization may be possible for the SUP05 symbionts given the considerably low $\delta^{15}N$ values in *O. pearseae* (average 1.6‰) and the successful amplification of the SUP05-related periplasmic nitrate reductase alpha subunit (*napA*) gene. The actual abundance of SUP05 symbionts per individual anemone is not known, nor is the regulation of carbon or nitrogen nutrient exchange, and thus the overall nutritional influence of the SUP05 bacteria is not yet quantifiable.

Finally, *Ostiactis pearseae* tissue $\delta^{34}S$ values (~-1‰) represented a large offset from typical marine biomass (16-21‰; Kaplan et al. 1963), where biogenic sulfur is sourced from seawater sulfate with minimal isotopic fractionation (21‰; Paris et al. 2013). The average $\delta^{34}S$ observed in *O. pearseae* tissues is consistent with typical hydrothermal vent fauna (-5 to +5‰; Fry et al. 1983), which are known to incorporate a local source of sulfur (e.g. volcanic, thermally-altered sulfur at ~0‰; Sakai et al. 1984; Canfield 2004) via internal symbioses or direct consumption of sulfide-oxidizing bacteria. However, several individuals of *O. pearseae* revealed even lower $\delta^{34}S$ values (down to -11‰), which would likely require the additional incorporation of substantial sulfide produced via microbial sulfate reduction, which is expected to have a $\delta^{34}S$ signature of -20‰ or lighter (Chambers & Trudinger 1979; Morse et al. 1987). The incorporation of sulfide sourced from dissimilatory sulfate reduction, rather than hydrothermal sulfide, has been similarly proposed for SUP05-hosting *Bathymodiolus* mussels from both Kakaijima Island and the Kaikata Caldera, which had tissue $\delta^{34}S$ values of -12‰ and -25‰, respectively, with a comparable tissue sulfur content of ~0.8% (n = only 1 specimen each; Kim et al. 1989; Yamanaka et al. 2000). The wide range of $\delta^{34}S$ values for *O. pearseae* tissues (~ -11 to 9‰), compared to other thiosymbiont-hosting animal species, could be due to a combination of traditional feeding by the host, variable sulfide oxidation by the SUP05 symbionts (e.g. utilization of H_2S, HS^-, or other reduced S species, including endogenous elemental sulfur), or variation in the sulfur sourced from the petroleum-rich sediments of the Pescadero Basin.

Many uncultivated candidate bacterial phyla have been discovered in recent years within a variety of environments (Rinke et al. 2013; Kantor et al. 2013; Harris et al. 2014). They usually have small genomes (<1 Mb) with dramatically reduced biosynthetic capabilities, and yet exist globally in both marine and terrestrial habitats (Wrighton et al. 2012). Several of these candidate phyla, known as the OD1 and BD1-5 groups (also referred to as Parcubacteria and Gracilibacteria, respectively), comprised up to 16-27% of the

Ostiactis pearseae bacterial community, and are known to play an important role in sulfur cycling (Wrighton et al. 2012). Nelson and Stegan (2015) proposed an ectosymbiotic or parasitic lifestyle for the OD1, given their inability to synthesize vitamins, amino acids, nucleotides, and fatty acids. Additionally, while most candidate phyla are found in anoxic habitats, some OD1 genomes contained genes suggestive of O_2 use as a terminal electron acceptor (Brown et al. 2015; Nelson and Stegan 2015). Although not previously associated with the sulfide-oxidizing SUP05 group, or any specific proteobacterial group, the role of OD1 in sulfur reduction (Wrighton et al. 2012) and their diverse repertoire for attachment and adhesion (Nelson and Stegan 2015) forecasts a possible direct association with either the SUP05 bacteria or *O. pearseae* mucous, for example.

Conclusion

Despite 40+ years of appreciation for chemosynthetic symbioses and the continued search for their occurrence in the most well-known habitats, Cnidaria have not been among the animals known to associate with chemoautotrophic bacteria. Here, we identify a hydrothermal vent sea anemone, *Ostiactis pearseae*, at 3700 m depth in the Pescadero Basin, Gulf of California, that appears to be nutritionally supported by internal chemoautotrophic bacteria. This species, one of only 2 dominant sessile animals observed on the vent chimneys, has an unusual life position, often located in and amongst vent-obligate siboglinid tubeworms, very near to actively venting fluids. *Ostiactis pearseae* houses putative sulfide-oxidizing SUP05 bacteria in its epidermis, with which it appears to have established a facultative nutritional symbiosis, based on a broad range of carbon, nitrogen, and sulfur isotopes. Facultative nutritional symbioses are often more difficult to recognize, compared to obligate alliances, but they are surely more common in nature (Goffredi et al. 2020), particularly in Cnidaria which experience symbiont gain and loss readily (ex. Jones et al. 2008; Larson et al. 2014; Vohsen et al. 2019). So, too, is the difficulty in uncovering nested symbioses, often involving microbe-microbe synergies. In this study, an unusual abundance of two candidate phyla, Parcubacteria and Gracilibacteria (a.k.a. OD1 and BD1-5, respectively) within *O. pearseae* tentacles, hints at the roles they may play in the cycling of nutrients within and on animal hosts. Cnidaria symbioses are considered foundational for coral reefs, and perhaps they also play an important role at hydrothermal vents. It would be worth investigating additional Anthozoa species observed to inhabit venting fluids at other sites worldwide (Doumenc & Van-Praët 1988; Sanamyan & Sanamyan 2007; Rogers et al. 2012), to see whether they have also forged nutritional relationships with chemosynthetic bacteria, such as the versatile SUP05 group.

Figure Legends

Figure 1: Locations and in situ images of the actiniarian *Ostiactis pearseae*
A. Location of South Pescadero Basin (SPB) vent fields Auka (in B) and JaichMaa 'ja'ag (in C). Inset shows location of SPB at the mouth of the Gulf of California between the tip of the Baja Peninsula and mainland Mexico. **B.** Auka vent field samples and chimneys. (samples symbolized as in C). **C.** JaichMaa 'ja'ag vent field samples and chimneys. Legend shows the sample types. Maps A,B, and C show 1-m resolution bathymetry collected by mapping AUVs (owned and operated by the Monterey Bay Aquarium Research Institute). Color ramps show the depth ranges. **D-F.** Specimens of *Ostiactis pearseae* collected from both vent fields (shown as yellow squares in B and C), indicated by arrows. **G.** An individual *O. pearseae* near to the chemosynthetic tubeworms *Riftia pachyptila* and *Oasisia* aff. *alvinae.*

Figure 2. *Ostiactis pearseae* external and internal anatomy, including cnidae
A-B. External anatomy of *Ostiactis pearseae* from Pescadero Basin; (A) lateral view; (B) oral view. **C.** Detail of distal row of papillae in the column (arrows). **D.** Detail of longitudinal section through perforated papillae (cinclide). **E.** Longitudinal section of distal column showing mesogleal marginal sphincter muscle (area within rectangle). **F.** Cross section of a tentacle showing ectodermal longitudinal muscles (arrows). **G.** Cross section at the actinopharynx level showing cycles of mesenteries; numbers between mesenteries indicate different cycles. **H.** Detail of marginal sphincter muscle fibers in the mesoglea. **J.** Detail of developing oocytes and lipid inclusions (red small dots) in the gastrovascular cavity. **I.** Detail of spermatic cysts (arrow points to largest cyst). **K.** Cnidae types of *O. pearseae*: basitrichs (a, c, e, h, k), holotrichs (b, f), robust spirocysts (d, g), *p*-mastigophores A (i, l), *p*-mastigophores B1 (j, m). Abbreviations: ep, epidermis; ga, gastrodermis; me, mesoglea; pap, papillae. Scale bars: A-C, 6 mm; D, G, 1 mm; E, 0.5 mm; F, H, I, J, 0.1 mm; K, 25 µm.

Figure 3. Phylogenetic placement of *Ostiactis pearseae*
Phylogenetic reconstruction resulting from maximum likelihood analysis using PhyML (RaxML results not shown, but congruent) of the concatenated dataset of three mitochondrial (12S rDNA, 16S rDNA, COIII) and a partial nuclear marker (18S rDNA). Doted boxes indicate actiniarian suborders; colored triangles and green box indicate actiniarian superfamilies; empty boxes and arrows indicate relevant actiniarian clades. Position of *Ostiactis pearseae* specimens from Pescadero Basin vent communities is highlighted in the orange box; the position of an additional sea anemone (unidentified morphospecies Kadosactinidae 'sp. B') is indicated by the light orange box. Bootstrap resampling values indicated above branches; only support values > 50% are shown.

Figure 4: ^{13}Carbon, ^{15}Nitrogen, ^{34}Sulfur isotope signatures for *Ostiactis pearseae* and comparison actiniarians

A. $\delta^{13}C$ and $\delta^{15}N$ values for the tentacles of *Ostiactis pearseae* from the Pescadero Basin vents, compared to neighboring anthozoans, including unidentified zoanthids ('zoan') and sea anemone (Kadosactinidae 'sp. B'). Data for Pescadero Basin actiniarians collected in 2015 (from Goffredi et al. 2017; red checkered triangles) as well as seep-associated corals from the Gulf of Mexico (Vohsen et al. 2020; purple circles) and unidentified anemones from Gorda Ridge hydrothermal vents (Van Dover & Fry 1994; purple squares) are also included. Data from Vohsen et al. 2020 was extracted from their Figure 7 using an online Web plot digitizer (http://arohatgi.info/WebPlotDigitizer/). **B.** $\delta^{34}S$ and tissue sulfide content (%, dry weight) values for the tentacles of *O. pearseae* from the Pescadero Basin vents, compared to neighboring Anthozoa, including an unidentified zoanthid ('zoan') and sea anemone (Kadosactinidae 'sp. B'). *Bathymodiolus aduloides* from muddy sediments off of Kakaijima Island taken from Yamanaka et al. 2000.

Figure 5: Relative abundance of 16S rRNA bacterial phylotypes, recovered from *Ostiactis pearseae* and comparison samples

A. Relative abundance of bacterial families from *Ostiactis pearseae* from the Pescadero Basin vents, compared to neighboring Anthozoa, including unidentified zoanthids ('zoan') and Kadosactinidae 'sp. B', nearby obligate vent tubeworms *Riftia pachyptila* and *Oasisia* aff. *alvinae*, and seawater. Each color on the graph represents a distinct family-level phylotype or lowest level available. The top 15 dominant family phylotypes are indicated in the key. For all others, see DataFile S1, including raw and processed data, as well as representative sequences for all dominant hits. **B.** Six distinct SUP05 OTUs (99% 16S rRNA sequence similarity) recovered from *O. pearseae*, compared to the surrounding seawater. The heatmap scale reflects the number of reads per sample. Phylogenetic relationships between the SUP05 OTUs are shown in Figure S1. See also DataFile S1, for representative sequences of each OTU. **C.** Non-metric multidimensional scaling (NMDS) ordination of microbial communities associated with *O. pearseae*, versus the other neighboring species and overlying seawater. Each point represents all 16S rRNA sequences recovered from a single specimen or sample. ANOSIM $p < 0.022$, suggesting a significant difference between *O. pearseae* and any other sample set (ex. other sea anemones, water samples; $R = 0.88\text{-}1.00$). HTV = hydrothermal vent. spB = another undescribed sea anemone (Kadosactinidae 'sp. B') from the Pescadero Basin. zoan = unidentified zoanthids from the Pescadero Basin.

Figure 6. Microscopy of the tentacles of *Ostiactis pearseae*

A. Whole specimen image - SO194-S2, SIO-BIC Co3067. **B.** light microscopy of 3-µm sections embedded in Steedman's resin, and **C-G**. fluorescent *in situ* signal amplification

via hybridization chain reaction-FISH (HCR-FISH) microscopy of *Ostiactis pearseae* tentacles. An unlabeled probe (Anem_SUP05), with a specific sequence initiator tag was designed to be an exact match to the putative thiotrophic symbiont (related to the SUP05 clade). This probe was then amplified via HCR-FISH using DNA hairpins labelled with Alexa488, shown in green. DAPI-stained nuclei of host cells are shown in blue. **F-G.** Bacteria can be seen within the epidermis, in and amongst nuclei, positioned just above or immediately adjacent to cnidocysts. **H-I**. Light microscopy of *O. pearseae* tentacles**. J-L**. Transmission electron (TEM) microscopy of *O. pearseae* tentacles. **I.** Bacteria are concentrated in the periphery of elongated epidermal cells (designated by the orange box, which corresponds to the area of TEM imagery), and positioned near cnidae, shown in pink arrowheads. No bacteria were observed in the mesogloea or gastrodermis. **J.** Close-up of bacteria near a cnidocyst capsule, with enclosed tubule. **K.** Close-up showing clear membranes surrounding the bacterial cells, designated by orange arrowheads. **L.** Arrowheads (in green) point to bacteria possibly being endocytized via clathrin-coated pits, as well as nearby clusters of bacterial cells within the elongated epidermal cells of *O. pearseae.* nu, nucleus. bac, bacteria. cni, cnidae. meso, mesoglea. gastro, gastrodermis. epi, epidermis. Scale bars are 5 mm (A), 2 mm (B), 50 µm (C), 1 µm (D), 10 µm (E-G), 250 µm (H), 25 µm (I), 1 µm (J-L).

Methods

Specimen Collections

All specimens and water samples were collected from active vent sites within the Pescadero Basin, Gulf of California (~ 3700 m depth), using the ROV *SuBastian* during the R/V *Falkor* expedition FK103118 (October-November 2018), specifically from six sites at two vent fields within ~2 km of each other; the previously described Auka vent field (refs) and a newly discovered JaichMaa 'ja'ag vent field (Fig. 1; Table 1). Sea anemones were collected by ROV manipulator or suction sampler (Supplemental video, currently available at https://doi.org/10.5061/dryad.mkkwh70wt) and preserved shipboard as described below in each analysis section. Targeted water samples (2 L) were collected via Niskin bottle mounted on ROV *SuBastian*.

Material examined for redescription of **Ostiactis pearseae**

SIO-BIC Co3060 [GC18-0004] (S0193-R2): Specimens: 2; Details: Fixative 4% paraformaldehyde; Preservative: 50% EtOH; Matterhorn, Auka Vent Field, Pescadero Basin, Mexico (23.95404°N, 108.86296°W); 3655 m; 14-Nov-2018. SIO-BIC Co3061 [GC18-0005] (S0193-A2): Specimens: 1; 10% formalin, preserved 50% EtOH; Matterhorn to Diane's Vent, Auka Vent Field, Pescadero Basin, Mexico (23.95472°N, -108.86233°W); 3655 m; 14-Nov-2018. SIO-BIC Co3067 [GC18-0028] (S0194-S2): Specimens: 2; fixed: 10% formalin; 50% EtOH; Z Mound, Auka Vent Field, Pescadero Basin, Mexico (23.95666°N, -108.86171°W); 3670 m; 15-Nov-2018. Material studied has been deposited in the Benthic Invertebrate Collection of Scripps Institution of Oceanography (University of California San Diego) and the Invertebrate Division collection of the American Museum of Natural History (AMNH) in New York.

Additional specimens examined in this study include Kadosactinidae ‘sp.B’ (SIO-BIC Co3065 [GC18-0012] (S0193-S4) and the unidentified zoanthid (SIO-BIC Co3066 [GC18-0025] (S0194-S1).

Carbon, nitrogen, and sulfur isotope analysis

Tissue samples were dissected at sea, rinsed in milli-Q water, and frozen at -20°C until thawed, washed with milli-Q water, and dried for 48 h at 60°C. Carbon and nitrogen isotope determinations of anemone tissues were made via isotope ratio mass spectrometry. Samples (0.2-0.8 mg dry weight) were loaded in tin boats and analyzed for total organic carbon (TOC) and total nitrogen (TN) abundances and $\delta^{13}C_{org}$ and $\delta^{15}N$ using a Flash 2000 Elemental Analyzer (Thermo Fisher Scientific) interfaced to a Delta V Plus IRMS (Thermo Fisher Scientific) at Washington University, Missouri, USA. Samples were interspersed with several replicates of both in-house standards and international reference materials, including: IAEA-CH-6, IAEA-CH-3, IAEA-NO3,

USGS-40, and USGS-41. TOC and TN abundances were quantified by integrating peak areas against those produced by in-house standards across a range of masses. The isotopic values are expressed in permil (‰) relative to international standards V-PDB (Vienna Pee Dee Belemnite) and Air for carbon and nitrogen, respectively. The long-term standard deviation is 0.2‰ for $\delta^{13}C_{org}$ and 0.3‰ for $\delta^{15}N$. Sulfur isotope analyses were performed by combusting ~2-5 mg (dry weight) of tissue using a Costech ECS 4010 elemental analyser coupled to a Thermo Fisher Scientific Delta V Plus mass spectrometer. Sulfur isotope values are expressed in standard delta notation ($\delta^{34}S$) in permil (‰) as a deviation from the Vienna Canyon Diablo Troilite (VCDT) standard. The long-term standard deviation is 0.3‰ for $\delta^{34}S$ is 0.3‰ based on in-house and international standards, including NBS-127 and IAEA-S1.

DNA extraction

Specimens for molecular analysis (Table 1) were preserved immediately upon collection in ~90% ethanol and stored at 4°C. Total genomic DNA was extracted from tissues using the Qiagen DNeasy kit (Qiagen, Valencia, CA, USA) according to the manufacturer's instructions. 2L water samples were filtered onto a 0.22 µm Sterivex-GP polyethersulfone filter (Millipore-Sigma, St. Louis, MO, USA) and frozen at -80°C until DNA analysis. DNA extraction from Sterivex PES filters was also performed using the Qiagen DNeasy kit, according to the manufacturer's instructions, with the exception of the first step where 2 ml of ATL lysis buffer was added to the Sterivex filter, via luer lock and syringe, and rotated at 56°C for 12 hours. This solution was recovered from the filter, also via luer lock and syringe, and processed as usual.

Molecular Analysis of the microbial community

A 1000-bp region of the gene coding for *napA* (periplasmic nitrate reductase) was amplified directly from *Ostiactis* tissues using the primers V16F (5′-GCNCCNTG-YMGNTTYTGYGG-3′) and V17R (5′-RTGYTGRTTRAANCCCATNGTCCA-3; Flanagan et al. 1999), while a 408 bp fragment of the *aprA* gene (subunit of particulate methane monooxygenase enzyme) was generated using primers, aps1F (5-TGGCAGATCATGATYMAYGG-3) and aps4R (5-GCGCCAACYGGRCCRTA-3, described in Blazejak et al. 2006). A 1465-bp fragment of the 16S rRNA gene was amplified using the primers 27F and 1492R. Annealing conditions of 50°C, 50°C and 54°C were used for *napA, aprA*, and 16SrRNA, respectively. Otherwise, all thermal protocols included the following steps: an initial 5 min denaturation at 94°C, then 1 min at 94°C, 1 min annealing step, and 1 min at 72°C, for 25 cycles, and a final 5 min extension at 72°C. Amplification products were sequenced directly using Sanger sequencing, via Laragen Inc., and submitted to GenBank (accession numbers XXXXXXX – TBD; currently available at https://doi.org/10.5061/dryad.mkkwh70wt). Close environmental and cultured relatives were chosen using top hits based on BLAST

(www.ncbi.nlm.nih.gov).

The V4-V5 region of the 16S rRNA gene was amplified using bacterial primers with Illumina (San Diego, CA, USA) adapters on the 5′ end 515F (5′-TCGTCGGC-AGCGTCAGATGTGTATAAGAGACAGGTGCCAGCMGCCGCGGTAA-3′) and 806R (5′-GTCTCGTGGGCTCGGAGATGTGTATAAGAGACAGGGACTACHV-GGGTWTCTAAT-3′) (Caporaso et al. 2011). The PCR reaction mix was set up in duplicate for each sample with Q5 Hot Start High-Fidelity 2x Master Mix (New England Biolabs, Ipswich, MA, USA) and annealing conditions of 54°C for 25 cycles. Duplicate PCR samples were then pooled and 2.5 µL of each product was barcoded with Illumina NexteraXT index 2 Primers that include unique 8-bp barcodes (P5 5'-AATGATACGGCGACCACCGAG-ATCTACAC-XXXXXXXX-TCGTCGGCAGCGTC-3' and P7 5'-CAAGCAGAA-GACGGCATACGAGAT-XXXXXXXX-GTCTCGTGGGCTCGG-3'). Secondary amplification with barcoded primers used conditions of 66°C annealing temperature and 10 cycles. Products were purified using Millipore-Sigma (St. Louis, MO, USA) MultiScreen Plate MSNU03010 with a vacuum manifold and quantified using Thermo-Fisher Scientific (Waltham, MA, USA) QuantIT PicoGreen dsDNA Assay Kit P11496 on the BioRad CFX96 Touch Real-Time PCR Detection System. Barcoded samples were combined in equimolar amounts into single tube and purified with Qiagen PCR Purification Kit 28104 before submission to Laragen (Culver City, CA, USA) for 2 x 250bp paired end analysis on the Illumina MiSeq platform with PhiX addition of 15-20%.

MiSeq 16S rRNA sequence data was processed in Quantitative Insights Into Microbial Ecology (v1.8.0). Raw sequence pairs were joined and quality-trimmed using the default parameters in QIIME. Sequences were clustered into *de novo* operational taxonomic units (OTUs) with 99% similarity using UCLUST open reference clustering protocol, and then, the most abundant sequence was chosen as representative for each *de novo* OTU. Taxonomic identification for each representative sequence was assigned using the Silva-119 database, clustered at 99% similarity. A threshold filter was used to remove any OTU that occurred below 0.01% in the combined samples dataset. Analyses are based on Bray-Curtis distances of fourth-root transformed data, which minimizes errors in the ordination due to PCR bias, while not sacrificing genuine differences between samples. Quantification and statistical analyses are described in the Results sections and figure legends. Comparisons were performed using ANOVA and statistical significance was declared at $P < 0.05$. Statistical analyses of beta diversity (e.g. ANOSIM) were performed with Primer E. The raw and processed Illumina 16S rRNA sequence data, as well as representative sequences, are available in DataFile S1 on the Dryad Digital Repository (https://doi.org/10.5061/dryad.mkkwh70wt).

***Molecular Analysis of the anemone host* Ostiactis pearseae**

Phylogenetic relationships were determined via sequencing of three mitochondrial markers, the 12S rRNA, 16S rRNA, and cytochrome oxidase III genes, and the partial nuclear 18S rRNA gene. An 862-bp product of the 12S rRNA gene was amplified via primers ANTMT12SF (5'-AGCCAC-ACTTTCACTGAAACAAGG-3') and ANTMT12SR (5'-GTTCCCYYWCYCTYA-CYATGTTACGAC-3') according to Chen and Yu 2000. A 473-bp product of the 16S rRNA gene was amplified via primers ANEM16SA (5'-CACTGACCGTGATAATG-TAGCGT-3') and ANEM16SB (5'-CCCCATGGTAGCTTTTATTCG-3') according to Geller and Walton 2001. Finally, a 721-bp product of the cytochrome oxidase III (COIII) gene was amplified via primers COIIIF (5'-CATTTAGTTGATCCTAGGCCTTGACC-3') and COIIIR (5'-CAAACCACATCTA-CAAAATGCCAATATC-3') according to Geller and Walton 2001. Finally, a 502-bp product of the 18S rRNA gene was amplified via primers 18S-3F (5'- GTTCGATTC-CGGAGAGGGA-3') and 18S-5R (5'-CTTGGCAAATGCTITCGC-3') according to Giribet et al. 1996. Annealing conditions of 55°C, 51.5°C, 51°C and 54°C were used for 12SrRNA, 16SrRNA, COIII, and 18S rRNA, respectively. Otherwise, all thermal protocols included the following steps: an initial 5 min denaturation at 94°C, then 1 min at 94°C, 1 min annealing step, and 1 min at 72°C, for 30 cycles, and a final 5 min extension at 72°C. Amplification products were sequenced directly using Sanger sequencing, via Laragen Inc., and submitted to GenBank (accession numbers xxxxx-xxxxx TBD, currently available at https://doi.org/10.5061/dryad.mkkwh70wt).

Newly generated DNA sequences for *Ostiactis pearseae* (and those for morphotype identified as Kadosactinidae sp.B. in this contribution) were combined and analyzed with the dataset by Gusmão et al. (2019) for each of the four markers (Table S2). Sequences for each marker were separately aligned in MAFFT v.7 (Katoh et al. 2013, 2017) using the following settings: Strategy, L-INS-I; Scoring matrix for nucleotide sequences, 200PAM/k = 2; Gap open penalty, 1.53; Offset value, 0.05. Alignments for each marker were analyzed separately and as a concatenated dataset (alignments available from the Dryad Digital Repository at https://doi.org/10.5061/dryad.mkkwh70wt). For each gene region, the best model of nucleotide substitution was chosen using the Akaike information criterion (AIC) on jModeltest2 (Guindon and Gascuel, 2003; Darriba et al. 2012) implemented on the CIPRES Portal (Miller et al., 2010). Maximum Likelihood (ML) analyses were performed using RAxML-NG v0.6.0 (Kozlov et al. 2018), using the appropriate model of nucleotide substitution for each gene partition (12S: GTR+I+G; 16S: TVM+G; COIII: TPM3uf+I+G; 18S: TIM2+I+G; 28S: GTR+I+G) in the combined alignment. The Majority Rule Criterion was used to assess clade support allowing bootstrapping to halt automatically (-autoMRE). All analyses were run with gaps treated as missing data.

***Morphology and cnidae analysis of the anemone host* Ostiactis pearseae**

Specimens were examined whole and dissected. Histological sections 5-10 µm thick were made from different body regions of two specimens using standard paraffin techniques and stained with Heidenhain Azan stain (Presnell and Schreibman, 1997). The distribution and size ranges of cnidae in the tissues was analyzed from six specimens using light DIC microscopy (1000x magnification, oil immersion). Twenty non-fired capsules of each cnida type (when possible) were photographed and measured at random. Cnidae size distribution offers information on the variability in capsule size for each type of nematocyst. We follow a nematocyst terminology that combines the classification of Weill (1934) modified by Carlgren (1940), thus differentiating 'basitrichs' from '*b*-mastigophores' with that of Schmidt (1969, 1972) which captures the underlying variation seen in 'rhabdoids' (see Gusmão et al., 2018 for more details). We include photographs of each type of nematocyst for reliable comparison across terminologies and taxa (see Fautin, 1988). Higher-level classification for Actiniaria follows Rodríguez et al. (2014).

Hybridization Chain Reaction-Fluorescent in-situ hybridization

Specimens for fluorescence in situ hybridization (FISH) microscopy were initially preserved in 4% sucrose-buffered paraformaldehyde (PFA) and kept at 4°C for 24-48 hours. These PFA-preserved specimens were then rinsed with 2× PBS, transferred to 70% ethanol, and stored at –20°C. Tissues were dissected and embedded in Steedman's wax (1 part cetyl alcohol: 9 parts polyethylene glycol (400) distearate, mixed at 60°C). An ethanol: wax gradient of 3:1, 2:1 and 1:1, and 100% wax, was used to embed the samples (1 h each treatment at 37°C). Embedded samples were sectioned at ~3 µm thickness using a Leica RM2125 microtome and placed on Superfrost Plus slides. The protocol and all solutions used for HCR-FISH were as specified by Molecular Technologies, Inc., and closely followed Choi et al. 2014. Sections were dewaxed in three 100% ethanol rinses, allowed to dry, and equilibrated in hybridization buffer (Molecular Technologies; 30% formamide, 5× sodium chloride, sodium citrate (SSC = 750 mM NaCl, 75 mM sodium citrate), 9 mM citric acid (pH 6.0), 0.1% Tween 20, 50 µg/mL heparin, 1× Denhardt's solution, 10% dextran sulfate), for 20 min at 37°C. Excess buffer was removed and sections were hybridized overnight in a humidification chamber at 37°C in hybridization buffer, to which was added a final concentration of 5 nM of an unlabeled DNA probe, designed to be an exact match to the *Ostiactis pearseae* SUP05 16S rRNA phylotype (Anem-SUP05, 5'-ACCATACTCTAGTTTGCCAG-3'), based on the probe, 'BangT-642', specific for the thiotrophic SUP05 symbiont in *Bathymodiolus* mussels (Duperron et al. 2005). A general bacterial probe set (Eub338-I-III) was also used as a positive control. These probes contained a specific sequence initiator tag (termed B1 and B3) that triggered the oligomerization of pairs of fluorescently-labeled DNA hairpins (i.e. the amplification step; Choi et al. 2014). The B1 initiator tag + linker

(5′-GAGGAGGGCAGCAAACGG-GAAGAGTCTTCCTTTACG-ATATT-3') was added to the 5′ end of the Anem-SUP05 probe. The B3 initiator tag + linker (5′-GTCCCTGCCTCTATATCTCCACTCAACTTT-AACCCG-ATATT-3′) was added to the 5′ end of each of three Eub338 probes I-III and to the Anem-SUP05 probe. In this case, tag B1 was paired with Alexa647-labelled hairpins, and tag B3 was paired with Alexa488-labelled hairpins.

Excess probe was removed by sequentially washing the slides for 15 min at 37°C in probe wash buffer (Molecular Technologies; 30% formamide, 5× SSC, 9 mM citric acid (pH 6.0), 0.1% Tween 20, 50 µg/mL heparin) to which 5× SSCT (750 mM NaCl, 75 mM sodium citrate, 0.1% Tween 20, pH 7) had been added to final concentrations (vol/vol) of 25%, 50%, and then 75%. This wash sequence was followed by two 15-min washes in 100% 5× SSCT at 37°C. Before amplification, 6 pmol of each hairpin, per reaction, was 'snap cooled' by heating to 95°C for 90 s, followed by 25°C for 30 min, in a thermocycler in separate PCR tubes. During this time, sections were equilibrated with amplification buffer (Molecular Technologies; 5× SSC, 0.1% Tween 20, 10% dextran sulfate) at room temperature for 30 min. For amplification, each 'snap-cooled' hairpin in a pair was added to 100 µl amplification buffer (for a final hairpin concentration of 60 nM for each amplifier hairpin), and then sections were incubated overnight (~18 h) at room temperature on a rocking platform protected from light. To remove unbound hairpin sequences, sections were washed twice in 5× SSCT for 15 min at room temperature, followed by two 30-min washes in 5× SSCT. Sections were rinsed with distilled water and counterstained with 4'6'-diamidino-2-phenylindole (DAPI, 5 mg/mL) for 1 min, rinsed again and mounted in Citifluor. Tissues were examined by epifluorescence microscopy using either a Nikon E80i epifluorescence microscope with a Nikon DS-Qi1Mc high-sensitivity monochrome digital camera or a Zeiss Elyra microscope with an ANDOR-iXon EMCCD camera.

Transmission electron microscopy

Specimens for TEM and semi-thin sectioning were fixed in PFA and preserved in 50% EtOH. Before embedding, specimens were rehydrated, post-fixed with 1% OsO_4 and subsequently dehydrated again in an ascending acetone series and embedded in araldite. 1 µm semi-thin sections were sectioned using a "Diatome Histo Jumbo" diamond knife on a Leica Ultracut S ultramicrotome and stained with toluidine blue (1% toluidine,1% sodium-tetraborate and 20% saccharose). Coverslips were mounted with araldite and sections were imaged with an Olympus microscope (BX-51) equipped with the dot.slide system (2.2 Olympus, Hamburg). Silver interference–colored sections (70 – 75 nm) were prepared using a "Diatome Ultra 45°" diamond knife. The sections were placed on Formvar-covered, single-slot copper grids and stained with 2% uranyl acetate and lead citrate in an automated TEM stainer (QG-3100, Boeckeler Instruments). Ultra-thin

sections were examined using a Zeiss EM10 transmission electron microscope with digital imaging plates (DITABIS Digital Biomedical Imaging Systems, Germany).

Declarations

Ethics approval and consent to participate

Not applicable

Consent for publication

Not applicable

Availability of Data and Materials

Longer partial length 16S rRNA and ITS sequences are available from GenBank under accession numbers XXXXXX-XXXXXX (TBD). The raw Illumina barcode sequence data and QIIME processed data are available in DataFile S1 from the Dryad Digital Repository (https://doi.org/10.5061/dryad.mkkwh70wt), along with representative sequences for the SUP05 OTUs. Alignments for the anemone 12S rRNA, 16S rRNA, 18S rRNA, and COIII for both *Ostiactis pearseae* and Kadosactinidae 'sp.B', used to generate Figure 3, are also available at https://doi.org/10.5061/dryad.mkkwh70wt. Animal images and specimens were vouchered for long-term archiving into the Benthic Invertebrate Collection at Scripps Institution of Oceanography (sioapps.ucsd.edu/collections/bi/).

Competing interests - TBD

The authors declare that they have no competing interests.

Funding

Support for SKG and CM was provided by a Faculty Enrichment Grant and the Undergraduate Research Center, respectively, through Occidental College. Support for ET was provided, in part, by a post-doctoral fellowship from the German Research Foundation (DFG TI 973/1-1). The research expedition FK181031 was made possible via support from the Schmidt Ocean Institute.

Authors' Contributions

S.K.G. conducted DNA analysis, including 16S rRNA barcoding, host gene sequencing, and fluorescent microscope analyses, analyzed experimental data, wrote the manuscript with input from coauthors, and participated in the research expedition. C.M. conducted DNA analysis, including 16S rRNA barcoding. E.T. performed electron microscopy analyses and participated in the research expedition. D.F. performed the isotope analyses and reviewed the paper. G.W.R. interpreted the electron microscopy analyses, advised on the species identification, and participated in the research expedition. L.G. conducted phylogenetic analysis and advised on host identification. E.R. conducted host anemone

815 analyses for species identification, including morphology, and wrote the manuscript. All
816 authors contributed to data interpretation and editing of the paper.
817
818 **Acknowledgements**
819 We thank the captain and crew of the R/V *Falkor*, *ROV SuBastian* pilots and technicians,
820 as well as scientific participants of FK181031, chief scientists R. Zierenberg, D. Caress,
821 and V. Orphan, as well as J. Paduan (MBARI) for Figure 1 maps and S. Connon for
822 assistance with microbial community analysis.

References

Blazejak A, Kuever J, Erséus C, Amann R, Dubilier N. Phylogeny of 16S rRNA, ribulose 1, 5-bisphosphate carboxylase/oxygenase, and adenosine 5′-phosphosulfate reductase genes from gamma-and alphaproteobacterial symbionts in gutless marine worms (Oligochaeta) from Bermuda and the Bahamas. Appl. Environ. Microbiol.. 2006 Aug 1;72(8):5527-36.

Breedy O, Rouse GW, Stabbins A, Cortes J, Cordes EE. New records of *Swiftia* (Cnidaria, Anthozoa, Octocorallia) from off the Pacific Costa Rican margin, including a new species from methane seeps. Zootaxa. 2019 Sep;4671(3):407-419.

Brown CT, Hug LA, Thomas BC, Sharon I, Castelle CJ, Singh A, Wilkins MJ, Wrighton KC, Williams KH, Banfield JF. Unusual biology across a group comprising more than 15% of domain Bacteria. Nature. 2015 Jul;523(7559):208-11.

Canfield, D.E., 2004. The evolution of the Earth surface sulfur reservoir. American Journal of Science, 304(10): 839-861.

Caporaso JG, Lauber CL, Walters WA, Berg-Lyons D, Lozupone CA, Turnbaugh PJ, Fierer N, Knight R. Global patterns of 16S rRNA diversity at a depth of millions of sequences per sample. Proceedings of the national academy of sciences. 2011 Mar 15;108(Supplement 1):4516-22.

Caress, D., Troni, G., Clague, D., Paduan, J., Martin, J., Thomas, H., Conlin, D., Martin, E, Meneses-Quiroz, E., Nieves-Cardoso, C., & Santa Rosa del Rio, M. 2015. Detection of active hydrothermal vent fields in the Pescadero Basin and on the Alarcón Rise using AUV multibeam and CTD data, Abstract OS23C-2027 presented at the AGU Fall Meeting, San Francisco, CA, December 14-18.

Carlgren, O. 1940. A contribution to the knowledge of the structure and distribution of the cnidae in the Anthozoa. Kungliga Fysiografiska Sällskapets Handlingar 51: 1–62.

Chambers LA, Trudinger PA. Microbiological fractionation of stable sulfur isotopes: a review and critique. Geomicrobiology Journal. 1979 Jan 1;1(3):249-93.

Chen CA, Yu JK. Universal primers for amplification of mitochondrial small subunit ribosomal RNA-encoding gene in scleractinian corals. Marine Biotechnology. 2000 Mar 1;2(2):146-53.

Choi HM, Beck VA, Pierce NA. Next-generation in situ hybridization chain reaction: higher gain, lower cost, greater durability. ACS nano. 2014 May 27;8(5):4284-94.

Daly M, Gusmão L. The first sea anemone (Cnidaria: Anthozoa: Actiniaria) from a whale fall. Journal of Natural History. 2007 Feb 16;41(1-4):1-1.

Daly M, Chaudhuri A, Gusmão L, Rodríguez E. Phylogenetic relationships among sea anemones (Cnidaria: Anthozoa: Actiniaria). Molecular phylogenetics and evolution. 2008 Jul 1;48(1):292-301.

Darriba, D., G.L. Taboada, R. Diallo, D. Posada. 2012. jModeltest 2: more models, new heuristics and parallel computing. Nature Methods 9: 772.

Doumenc D, Van-Prae ̈t M. 1988. Actinies abyssales d'un site hydrothermal du Pacifique

oriental. Oceanologica Acta, special 8:61 8.

Dubilier N, Bergin C, Lott C. Symbiotic diversity in marine animals: the art of harnessing chemosynthesis. Nature Reviews Microbiology. 2008 Oct;6(10):725-40.

Duperron S, Nadalig T, Caprais JC, Sibuet M, Fiala-Médioni A, Amann R, Dubilier N. Dual symbiosis in a *Bathymodiolus* sp. mussel from a methane seep on the Gabon continental margin (Southeast Atlantic): 16S rRNA phylogeny and distribution of the symbionts in gills. Appl. Environ. Microbiol.. 2005 Apr 1;71(4):1694-700.

Fautin, D.G. 1988. The importance of nematocysts to actiniarian taxonomy. *In* D.A. Hessinger and H.M. Lenhoff (editors), The biology of nematocysts: 487–500. New York: Academic Press.

Fautin DG, Mariscal RN. Cnidaria: anthozoa. New York: Wiley-Liss; 1991.

Fisher CR, Childress JJ, Minnich E. Autotrophic carbon fixation by the chemoautotrophic symbionts of *Riftia pachyptila*. The Biological Bulletin. 1989 Dec;177(3):372-85.

Flanagan DA, Gregory LG, Carter JP, Karakas-Sen A, Richardson DJ, Spiro S. Detection of genes for periplasmic nitrate reductase in nitrate respiring bacteria and in community DNA. FEMS Microbiology Letters. 1999 Aug 1;177(2):263-70.

Fujiwara Y, Takai K, Uematsu K, Tsuchida S, Hunt JC, Hashimoto J. Phylogenetic characterization of endosymbionts in three hydrothermal vent mussels: influence on host distributions. Marine Ecology Progress Series. 2000 Dec 8;208:147-55.

Geller JB, Walton ED. Breaking up and getting together: evolution of symbiosis and cloning by fission in sea anemones (genus *Anthopleura*). Evolution. 2001 Sep;55(9):1781-94.

Giribet G, Carranza S, Baguna J, Riutort M, Ribera C. First molecular evidence for the existence of a Tardigrada+ Arthropoda clade. Molecular biology and evolution. 1996 Jan 1;13(1):76-84.

Glaubitz S, Kießlich K, Meeske C, Labrenz M, Jürgens K. SUP05 dominates the gammaproteobacterial sulfur oxidizer assemblages in pelagic redoxclines of the central Baltic and Black Seas. Appl. Environ. Microbiol.. 2013 Apr 15;79(8):2767-76.

Goffredi SK, Childress JJ, Desaulniers NT, Lallier FJ. Sulfide acquisition by the vent worm *Riftia pachyptila* appears to be via uptake of HS-, rather than H2S. Journal of Experimental Biology. 1997 Oct 1;200(20):2609-16.

Goffredi SK, Johnson S, Tunnicliffe V, Caress D, Clague D, Escobar E, Lundsten L, Paduan JB, Rouse G, Salcedo DL, Soto LA. Hydrothermal vent fields discovered in the southern Gulf of California clarify role of habitat in augmenting regional diversity. Proceedings of the Royal Society B: Biological Sciences. 2017 Jul 26;284(1859):20170817.

Goffredi SK, Tilic E, Mullin SW, Dawson KS, Keller A, Lee RW, Wu F, Levin LA, Rouse GW, Cordes EE, Orphan VJ. Methanotrophic bacterial symbionts fuel dense populations of deep-sea feather duster worms (Sabellida, Annelida) and extend the spatial influence of methane seepage. Science Advances. 2020 Apr 1;6(14):eaay8562.

Grajales A, Rodríguez E Elucidating diversity within the Aiptasiidae, a widespread cnidarian-dinoflagellate model system (Cnidaria: Anthozoa: Actiniaria: Metridioidea). Molecular Phylogenetics and Evolution. 2016;94(A):252-263.

Gruber-Vodicka HR, Leisch N, Kleiner M, Hinzke T, Liebeke M, McFall-Ngai M, Hadfield MG, Dubilier N. Two intracellular and cell type-specific bacterial symbionts in the placozoan Trichoplax H2. Nature microbiology. 2019 Sep;4(9):1465-74.

Guindon, S. & Gascuel, O. A simple, fast, and accurate algorithm to estimate large phylogenies by maximum likelihood. *Syst. Biol.* **52**, 696–704 (2003).

Guindon, S, J.F. Dufayard, V. Lefort, M. Anisimova, W. Hordijk, and O. Gascuel. 2010. New algorithms and methods to estimate maximum-likelihood phylogenies: assessing the performance of PhyML 3.0. Systematic Biology 59: 307–321.

Gusmão, L.C., A. Grajales, and E. Rodríguez. 2018. Sea Anemones through X-rays: Visualization of Two Species of *Diadumene* (Cnidaria, Actiniaria) Using Micro-CT. American Museum Novitates 3907: 1–45.

Gusmão LC, Rodríguez E, Daly M (2019) Description of *Calliactis tigris* sp. nov.: reconciling taxonomy and phylogeny in hermit-crab symbiotic anemones (Cnidaria: Actiniaria: Hormathiidae). Organismal Diversity and Evolution, 19(4): 567-583; doi.org/10.1007/s13127-019-00414-2.

Harris JK, Kelley ST, Pace NR. New perspective on uncultured bacterial phylogenetic division OP11. Appl. Environ. Microbiol.. 2004 Feb 1;70(2):845-9.

Hatch AS, Liew H, Hourdez S, Rouse GW. Hungry scale worms: Phylogenetics of Peinaleopolynoe (Polynoidae, Annelida), with four new species. ZooKeys. 2020 Dec 5;932:27.

Heijs SK, Sinninghe Damsté JS, Forney LJ. Characterization of a deep-sea microbial mat from an active cold seep at the Milano mud volcano in the Eastern Mediterranean Sea. FEMS microbiology ecology. 2005 Sep 1;54(1):47-56.

Ikuta T, Takaki Y, Nagai Y, Shimamura S, Tsuda M, Kawagucci S, Aoki Y, Inoue K, Teruya M, Satou K, Teruya K. Heterogeneous composition of key metabolic gene clusters in a vent mussel symbiont population. The ISME journal. 2016 Apr;10(4):990-1001.

Jones AM, Berkelmans R, van Oppen MJ, Mieog JC, Sinclair W. A community change in the algal endosymbionts of a scleractinian coral following a natural bleaching event: field evidence of acclimatization. Proceedings of the Royal Society B: Biological Sciences. 2008 Jun 22;275(1641):1359-65.

Kantor RS, Wrighton KC, Handley KM, Sharon I, Hug LA, Castelle CJ, Thomas BC, Banfield JF. Small genomes and sparse metabolisms of sediment-associated bacteria from four candidate phyla. MBio. 2013 Nov 1;4(5):e00708-13.

Kaplan, I.R., Emery, K.O., Rittenberg, S.C., 1963. The distribution and isotopic abundance of sulphur in recent marine sediments off southern California. Geochim. et Cosmochim. Acta, 27: 297 - 331.

970 Katoh, K., and D.M. Standley. 2013. MAFFT Multiple Sequence Alignment Software Version 7:
971 Improvements in Performance and Usability. Molecular Biology and Evolution 30: 772–780.
972
973 Katoh, K., J. Rozewicki, and K.D. Yamada. 2017. MAFFT online service: multiple sequence
974 alignment, interactive sequence choice and visualization. Brief in Bioinformatics
975 [doi:10.1093/bib/bbx108]
976
977 Kim ES, Sakai H, Hashimoto J, Yanagisawa F, Ohta S. Sulfur isotopic ratios of hydrothermal
978 vent-animals at Ogasawara Arc and Mid-Okinawa Trough-evidence for microbial origin of
979 hydrogen sulfide at low-temperature submarine hydrothermal areas. Geochemical journal.
980 1989;23(4):195-208.
981
982 Kozlov, A.M., D. Darriba, T. Flouri, B. Morel, and A. Stamatakis. 2018. RAxML-NG: a fast
983 scalable, and user-friendly tool for maximum likelihood phylogenetic inference. Bioinformatics
984 btz305. [doi:10.1101/447110]
985
986 Labrenz M, Jost G, Jürgens K. Distribution of abundant prokaryotic organisms in the water
987 column of the central Baltic Sea with an oxic–anoxic interface. Aquatic microbial ecology. 2007
988 Feb 2;46(2):177-90.
989
990 LaJeunesse TC, Parkinson JE, Gabrielson PW, Jeong HJ, Reimer JD, Voolstra CR, Santos SR.
991 Systematic revision of Symbiodiniaceae highlights the antiquity and diversity of coral
992 endosymbionts. Current Biology. 2018 Aug 20;28(16):2570-80.
993
994 Larson HK, Goffredi SK, Parra EL, Vargas O, Pinto-Tomas AA, McGlynn TP. Distribution and
995 dietary regulation of an associated facultative Rhizobiales-related bacterium in the omnivorous
996 giant tropical ant, *Paraponera clavata.* Naturwissenschaften. 2014 May 1;101(5):397-406.
997
998 Lefort, V., J. Longueville, and O. Gascuel. 2017. SMS: Smart Model Selection in PhyML.
999 Molecular Biology and Evolution 34: 24221–2424.
1000
1001 Levin LA, Orphan VJ, Rouse GW, Rathburn AE, Ussler III W, Cook GS, Goffredi SK, Perez
1002 EM, Waren A, Grupe BM, Chadwick G. A hydrothermal seep on the Costa Rica margin: middle
1003 ground in a continuum of reducing ecosystems. Proceedings of the Royal Society B: Biological
1004 Sciences. 2012 Jul 7;279(1738):2580-8.
1005
1006 Marlow HQ, Martindale MQ. Embryonic development in two species of scleractinian coral
1007 embryos: *Symbiodinium* localization and mode of gastrulation. Evolution & development. 2007
1008 Jul;9(4):355-67.
1009
1010 Marshall KT, Morris RM. Isolation of an aerobic sulfur oxidizer from the SUP05/Arctic96BD-19
1011 clade. The ISME journal. 2013 Feb;7(2):452-5.
1012
1013 McKiness ZP, Cavanaugh CM. The ubiquitous mussel: *Bathymodiolus aff. brevior* symbiosis at
1014 the Central Indian Ridge hydrothermal vents. Marine Ecology Progress Series. 2005 Jun
1015 23;295:183-90.
1016
1017 McAuley PJ. Regulation of numbers of symbiotic *Chlorella* in digestive cells of green hydra.
1018 Endocyt. Cell Res. 1985 Nov 1;2:179-90.
1019

McCowin MF, Feehery C, Rouse GW: Spanning the depths and depth-stratified: Three new species of *Bathymodiolus* (Bivalvia, Mytilidae) at seeps along the Costa Rica margin. Deep-Sea Research Part I 2020. In press.

Mellas RE, McIlroy SE, Fitt WK, Coffroth MA. Variation in symbiont uptake in the early ontogeny of the upside-down jellyfish, *Cassiopea* spp. Journal of experimental marine biology and ecology. 2014 Oct 1;459:38-44.

Miller, M.A., W. Pfeiffer, and T. Schwartz. 2010. Creating the CIPRES Science Gateway for inference of large phylogenetic trees. Proceedings of the Gateway Computing Environments Workshop (GCE): 1–8.

Morse JW, Millero FJ, Cornwell JC, Rickard D. The chemistry of the hydrogen sulfide and iron sulfide systems in natural waters. Earth-science reviews. 1987 Mar 1;24(1):1-42.

Neave MJ, Apprill A, Ferrier-Pagès C, Voolstra CR. Diversity and function of prevalent symbiotic marine bacteria in the genus *Endozoicomonas*. Applied microbiology and biotechnology. 2016 Oct 1;100(19):8315-24.

Nelson WC, Stegen JC. The reduced genomes of Parcubacteria (OD1) contain signatures of a symbiotic lifestyle. Frontiers in microbiology. 2015 Jul 21;6:713.

Paduan JB, Zierenberg RA, Clague DA, Spelz RM, Caress DW, Troni G, Thomas H, Glessner J, Lilley MD, Lorenson T, Lupton J. Discovery of hydrothermal vent fields on Alarcón Rise and in Southern Pescadero Basin, Gulf of California. Geochemistry, Geophysics, Geosystems. 2018 Dec;19(12):4788-819.

Palincsar EE, Jones WR, Palincsar JS, Glogowski MA, Mastro JL. Bacterial aggregates within the epidermis of the sea anemone *Aiptasia pallida*. The Biological Bulletin. 1989 Aug;177(1):130-40.

Paris G, Sessions AL, Subhas AV, Adkins JF. MC-ICP-MS measurement of δ34S andΔ 33S in small amounts of dissolved sulfate. Chemical Geology. 2013 May 8;345:50-61.

Petersen JM, Wentrup C, Verna C, Knittel K, Dubilier N. Origins and evolutionary flexibility of chemosynthetic symbionts from deep-sea animals. The Biological Bulletin. 2012 Aug;223(1):123-37.

Preheim SP, Boucher Y, Wildschutte H, David LA, Veneziano D, Alm EJ, Polz MF. Metapopulation structure of Vibrionaceae among coastal marine invertebrates. Environmental Microbiology. 2011 Jan;13(1):265-75.

Presnell, J.K., and M.P. Schreibman. 1997. Humason's animal tissue techniques. Baltimore, MD: Johns Hopkins University Press.

Rinke C, Schwientek P, Sczyrba A, Ivanova NN, Anderson IJ, Cheng JF, Darling A, Malfatti S, Swan BK, Gies EA, Dodsworth JA. Insights into the phylogeny and coding potential of microbial dark matter. Nature. 2013 Jul;499(7459):431-7.

1069 Robidart JC, Bench SR, Feldman RA, Novoradovsky A, Podell SB, Gaasterland T, Allen EE,
1070 Felbeck H. Metabolic versatility of the *Riftia pachyptila* endosymbiont revealed through
1071 metagenomics. Environmental Microbiology. 2008 Mar;10(3):727-37.
1072
1073 Rodríguez, E., M. Barbeitos, M. Daly, L.C. Gusmão, and V. Häussermann. 2012. Toward a
1074 natural classification: phylogeny of acontiate sea anemones (Cnidaria, Anthozoa, Actiniaria).
1075 Cladistics 1: 1–18.
1076
1077 Rodríguez, E., M.S. Barbeitos, M.R. Brugler, L.M. Crowley, A. Grajales, L. Gusmão, V.
1078 Häussermann, A. Reft, and M. Daly. 2014. Hidden among sea anemones: first comprehensive
1079 phylogenetic reconstruction of the order Actiniaria (Cnidaria: Anthozoa: Hexacorallia) reveals a
1080 novel group of hexacorals. PLoS ONE 9: 1–15.
1081
1082 Rogers AD, Tyler PA, Connelly DP, Copley JT, James R, Larter RD, Linse K, Mills RA,
1083 Garabato AN, Pancost RD, Pearce DA. The discovery of new deep-sea hydrothermal vent
1084 communities in the Southern Ocean and implications for biogeography. PLoS Biol. 2012 Jan
1085 3;10(1):e1001234.
1086
1087 Rouse GW, Wilson NG, Carvajal JI, Vrijenhoek RC. New deep-sea species of *Xenoturbella* and
1088 the position of Xenacoelomorpha. Nature. 2016 Feb;530(7588):94-7.
1089
1090 Sakai H, Des Marais DJ, Ueda A, Moore JG. Concentrations and isotope ratios of carbon,
1091 nitrogen and sulfur in ocean-floor basalts. Geochimica et Cosmochimica Acta. 1984 Dec
1092 1;48(12):2433-41.
1093
1094 Salcedo DL, Soto LA, Paduan JB. Trophic structure of the macrofauna associated to deep-vents
1095 of the southern Gulf of California: Pescadero Basin and Pescadero Transform Fault. PloS one.
1096 2019;14(11).
1097
1098 Sanamyan NP, Sanamyan KE. 2007. Deep-water Actiniaria from East Pacific hydrothermal vents
1099 and cold seeps. Invertebrate Zoology 4:83-102.
1100
1101 Schlichter, D. The importance of dissolved organic compounds in sea water for the nutrition of
1102 Anemonia sulcate Pennant(Coelenterata). Proc. Eur. Mar. Biol. Symp. 1975; 9: 395–405.
1103
1104 Schlichter, D. Adaptation of cnidarians for integumentary absorption of dissolved organic
1105 material. Rev. Can. Biol.1980; 39: 259-282.
1106
1107 Schmidt, H. 1969. Die Nesselkapseln der Aktinien und ihre differentialdiagnostische Bedeutung.
1108 Helgoländer Wissenschaftliche Meeresuntersuchungen 19: 284–317.
1109
1110 Schmidt, H. 1972. Die Nesselkapseln der Anthozoen und ihre Bedeutung fur die phylogenetische
1111 Systematik. Helgoländer Wissenschaftliche Meeresuntersuchungen 23: 422–458.
1112
1113 Schuett C, Doepke H, Grathoff A, Gedde M. Bacterial aggregates in the tentacles of the sea
1114 anemone *Metridium senile*. Helgoland Marine Research. 2007 Sep 1;61(3):211-6.
1115
1116 Shah V, Zhao X, Lundeen RA, Ingalls AE, Nicastro D, Morris RM. Morphological Plasticity in a
1117 Sulfur-Oxidizing Marine Bacterium from the SUP05 Clade Enhances Dark Carbon Fixation.
1118 mBio. 2019 Jun 25;10(3):e00216-19.
1119

Sunamura M, Higashi Y, Miyako C, Ishibashi JI, Maruyama A. Two bacteria phylotypes are predominant in the Suiyo Seamount hydrothermal plume. Appl. Environ. Microbiol.. 2004 Feb 1;70(2):1190-8.

Tait E, Carman M, Sievert SM. Phylogenetic diversity of bacteria associated with ascidians in Eel Pond (Woods Hole, Massachusetts, USA). Journal of experimental marine biology and ecology. 2007 Mar 26;342(1):138-46.

Ulloa O, Canfield DE, DeLong EF, Letelier RM, Stewart FJ. Microbial oceanography of anoxic oxygen minimum zones. Proceedings of the National Academy of Sciences. 2012 Oct 2;109(40):15996-6003.

Van Dover CL, Fry B. Stable isotopic compositions of hydrothermal vent organisms. Marine Biology. 1989 Aug 1;102(2):257-63.

Van Dover CL, Fry B. Microorganisms as food resources at deep-sea hydrothermal vents. Limnology and Oceanography. 1994 Jan;39(1):51-7.

Vohsen SA, Gruber-Vodicka HR, Osman EO, Saxton MA, Joye SB, Dubilier N, Fisher CR, Baums IB. Deep-sea corals near cold seeps associate with chemoautotrophic bacteria that are related to the symbionts of cold seep and hydrothermal vent mussels. bioRxiv. 2020 Jan 1.

Walsh DA, Zaikova E, Howes CG, Song YC, Wright JJ, Tringe SG, Tortell PD, Hallam SJ. Metagenome of a versatile chemolithoautotroph from expanding oceanic dead zones. Science. 2009 Oct 23;326(5952):578-82.

Weill, R. 1934. Contribution à l'Étude des Cnidaires et de leurs Nématocystes. Paris: Les Presses Universitaires de France.

Wrighton KC, Thomas BC, Sharon I, Miller CS, Castelle CJ, VerBerkmoes NC. Wilkins 475 MJ, Hettich RL, Lipton MS, Williams KH, Long PE, Banfield JF. 2012. Fermentation, 476 hydrogen, and sulfur metabolism in multiple uncultivated bacterial phyla. Science.;337:1661-5.

Yamanaka T, Mizota C, Maki Y, Fujikura K, Chiba H. Sulfur isotope composition of soft tissues of deep-sea mussels, Bathymodiolus spp., in Japanese waters. Benthos Research. 2000 Dec 31;55(2):63-8.

Yamanaka T, Mizota C, Fujiwara Y, Chiba H, Hashimoto J, Gamo T, Okudaira T. Sulphur-isotopic composition of the deep-sea mussel Bathymodiolus marisindicus from currently active hydrothermal vents in the Indian Ocean. Journal of the Marine Biological Association of the United Kingdom. 2003 Aug;83(4):841-8.

Zelnio K, Rodríguez E, Daly M. 2009. Hexacorals (Anthozoa: Actiniaria, Zoanthidea) from hydrothermal vents in the South-western Pacific. Marine Biology Research 5(6):547-57.

Table 1: Sample locations within the Pescadero Basin, Gulf of California, along with dive information, depth, and specimen descriptions for Anthozoa other than *Ostiactis pearseae*.

Ostiactis pearseae				
Auka vent field	**Dive #-Sample #**	**Depth**	**Lat**	**Lon**
Matterhorn[1]	S0193-R2	-3655	23°57.24218 N	108°51.77758 W
E. of Diane's vent	S0193-A2	-3655	23°57.28307 N	108°51.73963 W
Z vent (top)[1]	S0194-S2	-3670	23°57.39937 N	108°51.70276 W
S. of Z vent (small chimney)	S0200-R2w	-3687	23°57.36546 N	108°51.71477 W
JaichMaa 'ja'ag vent field				
Abuelita[1]	S0197-S2	-3692	23°56.53971 N	108°51.34850 W
Weey 'kual	S0199-S8	-3674	23°56.42347 N	108°51.35257 W
Water samples[2]				
Auka vent field	**Dive #-Sample #**	**Depth**	**Lat**	**Lon**
E. of Diane's vent	S0193-N2	-3642	23°57.29596 N	108°51.77752 W
JaichMaa 'ja'ag vent field				
Abuelita	S0197-N2	-3693	23°56.53998 N	108°51.35074 W
Weey 'kual	S0199-N1	-3669	23°56.41838 N	108°51.34473 W
Other Anthozoa[3]				
Auka vent field	**Dive #-Sample #**	**Depth**	**Description**	
Matterhorn	S0193-S4	-3655	Kadosactinidae 'sp.B' Green tentacles	
E. of Diane's vent	S0193-R3	-3655	Unidentified zoanthid	
Z vent (lower on structure)	S0194-R1	-3670	Unidentified zoanthid	
NW. of Z vent (diffuse flow)	S0194-R2	-3687	Unidentified zoanthid	
NW. of Z vent (diffuse flow)	S0194-S1	-3687	Unidentified zoanthid	
S. of Z vent (small chimney)	S0200-R2r	-3692	Kadosactinidae 'sp.B' Red tentacles	

[1] anemones collected very near active *Oasisia* tubeworms

[2] collected via Niskin sampler aboard the ROV SuBastian

[3] collected in the same general venting structure as *O. pearseae*, geo-locations noted above

Table 2. Size ranges of the cnidae capsules of *Ostiactis pearseae* (Daly & Gusmão, 2007). N: total number of capsules measured. F: Frequency, +++ = very common, ++ = common, + = rather common, * = sporadic.

Categories	Range length × width (µm)	Avg ± SD	N	S	F	Range length × width (µm)[3]
COLUMN [1]						
Basitrichs	17.2-26.0 x 2.6-4.4	21.7±2.3 x 3.4±0.3	122	6/6	++	13.1–22.5 x 1.9–3.0
Holotrichs	16.9-24.7 x 4.8-8.6	21.5±2.0 x 6.4±0.8	67	4/6	*/++	16.6–27.0 x 3.5–5.5
p-mastigophores B1	----	-----		0/6		17.8–33.9 x 2.6–5.3
TENTACLES						
Robust spirocysts	15.9-41.9 x 4.2-8.8	26.0±6.1 x 5.7±1.0	85	5/5	++	16.3–35.5 x 2.1–5.8
Basitrichs	15.2-33.2 x 2.3-4.3	23.3±4.0 x 3.5±0.5	113	5/5	+++	16.2–29.8 x 2.2–4.6
Holotrichs	15.6-28.5 x 4.0-9.3	23.3±2.7 x 7.1±1.0	79	5/5	+	23.1–34.4 x 2.9–6.9
ACTINOPHARYNX						
Basitrichs 1	16.4-20.2 x 2.6-3.2	18.1±1.7 x 2.9±0.2	5	2/3	*	16.8–26.3 x 2.0–3.3
Basitrichs 2	23.7-34.0 x 3.3-4.6	27.9±2.8 x 4.0±0.4	20	2/3	++	25.6–44.5 x 3.0–4.3
p-mastigophores A[2]	23.3-38.1 x 4.7-6.9	30.7±3.5 x 5.7±0.5	53	3/3	++	-----
p-mastigophores B1[2]	14.5-19.5 x 4.0-5.2	17.8±1.7 x 4.5±0.4	13	3/3	++	22.0–37.0 x 3.9–6.2
FILAMENTS						
Basitrichs	15.3-23.3 x 2.5-3.5	18.5±1.6 x 3.0±0.2	50	4/4	*/+	14.1–22.5 x 1.8–2.9
p-mastigophores A[2]	26.5-37.8 x 4.8-6.7	32.8±2.2 x 5.7±0.5	49	4/4	+	
p-mastigophores B1[2]	13.4-21.3 x 3.6-6.3	17.4±1.7 x 4.6±0.6	59	4/4	+++	17.5–37.6 x 3.4–6.0

[1]Two specimens with papillae in distal column (see Fig. 2); papillae with only basitrichs of similar sizes than those in the rest of the column (i.e. 17.0-21.6 x 2.7-3.7 µm).
[2]Categories pooled together as microbasic *p*-mastigophores in Daly & Gusmão (2007).
[3]Data from Daly & Gusmão (2007).

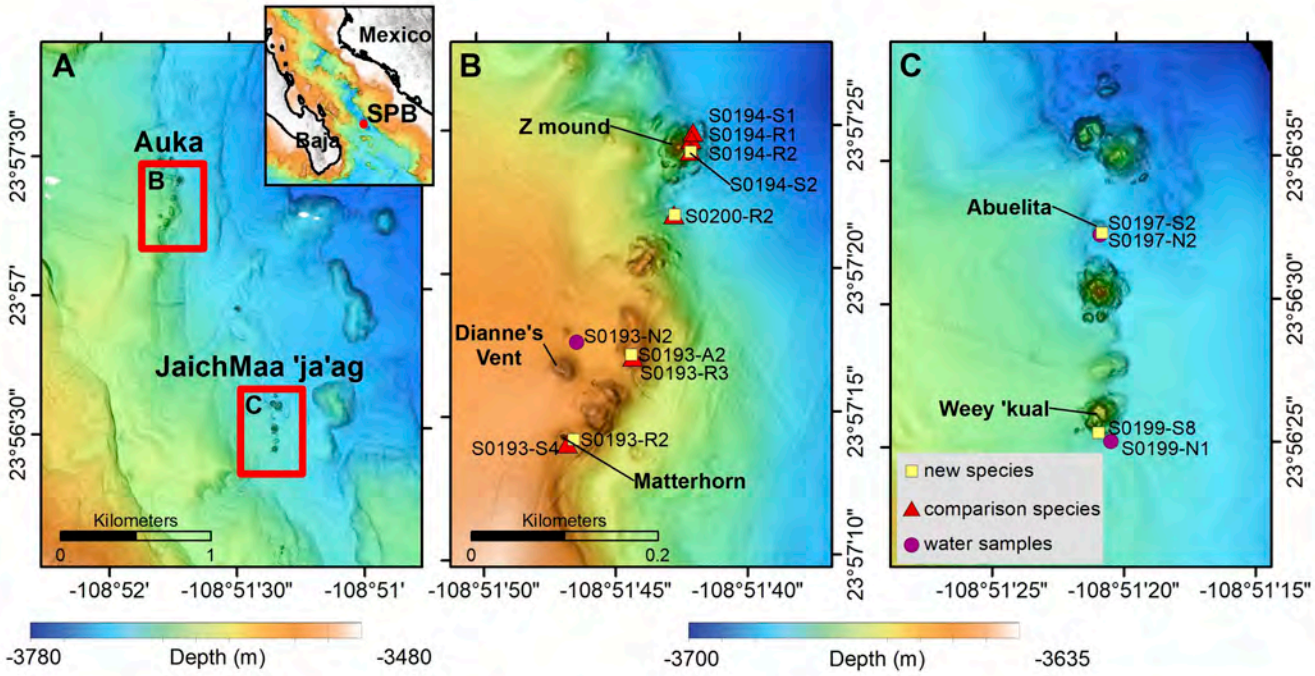

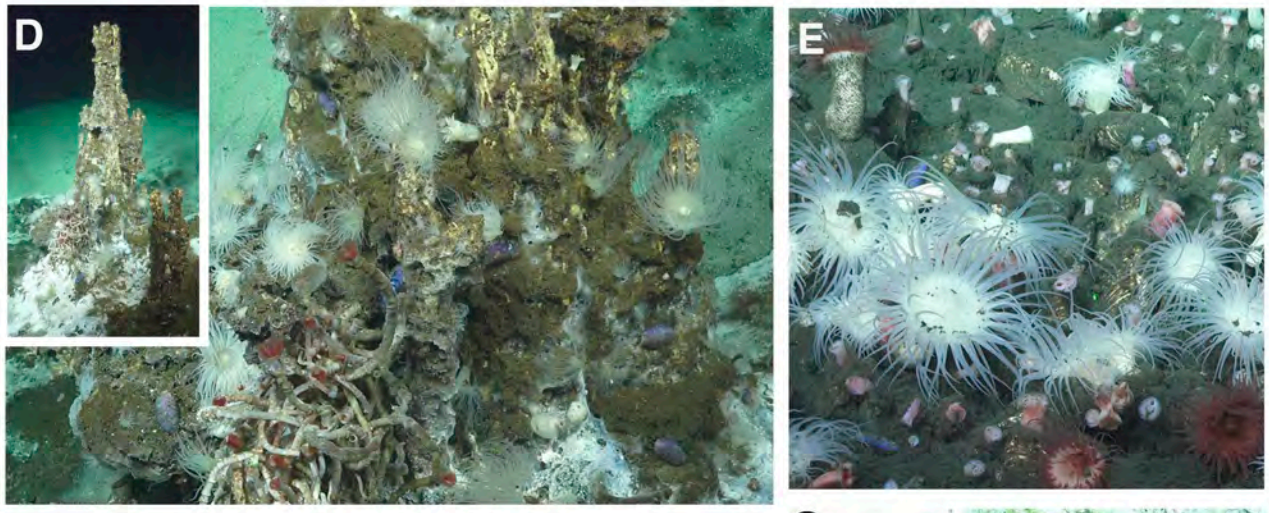

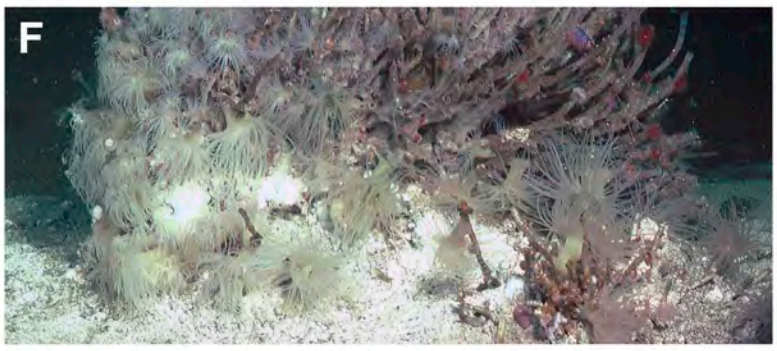

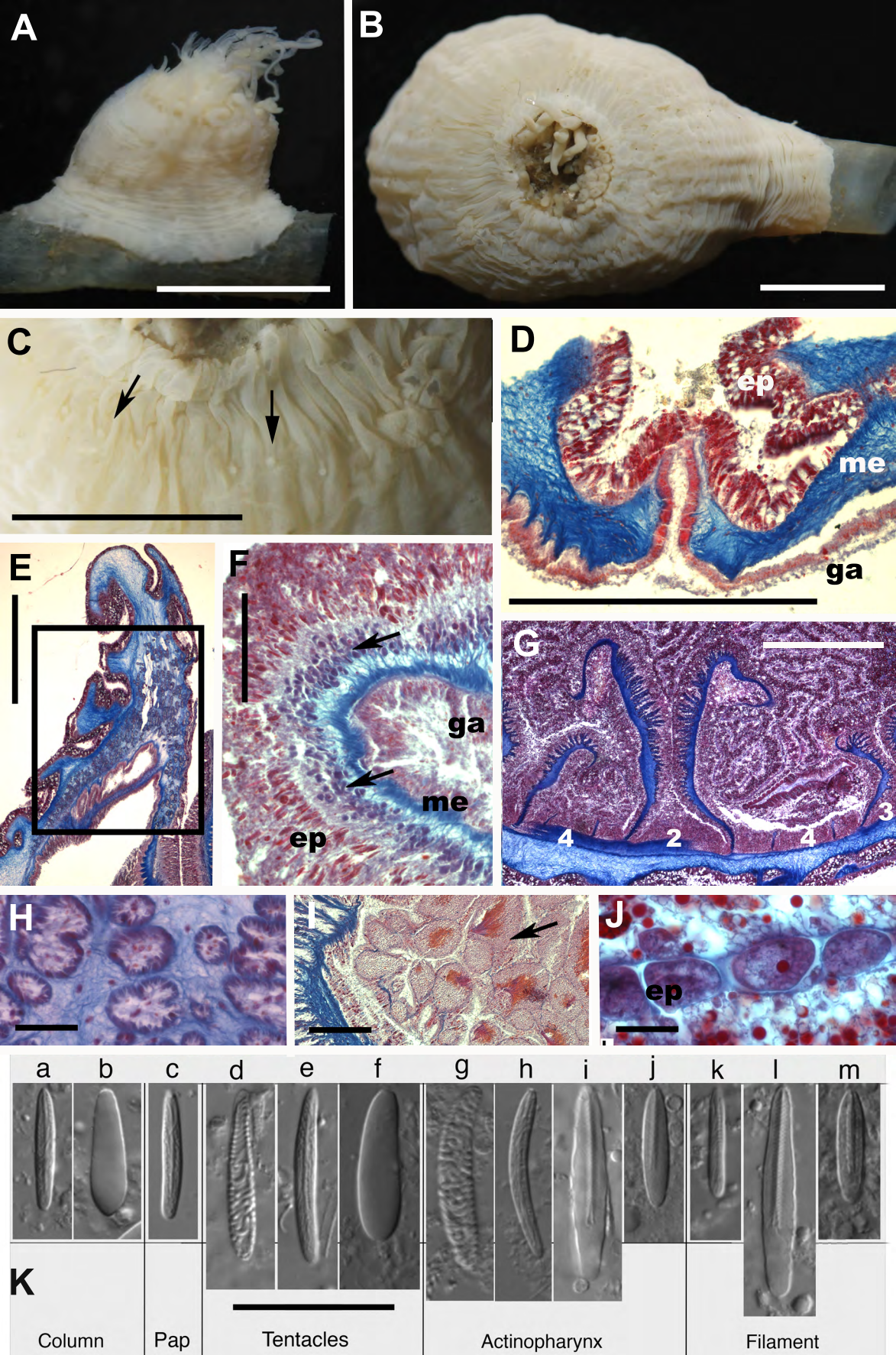
A
B
C
D
ep
me
ga
E
F
ga
me
ep
G
4
2
4
3
H
I
J
ep
a
b
c
d
e
f
g
h
i
j
k
l
m
K
Column
Pap
Tentacles
Actinopharynx
Filament

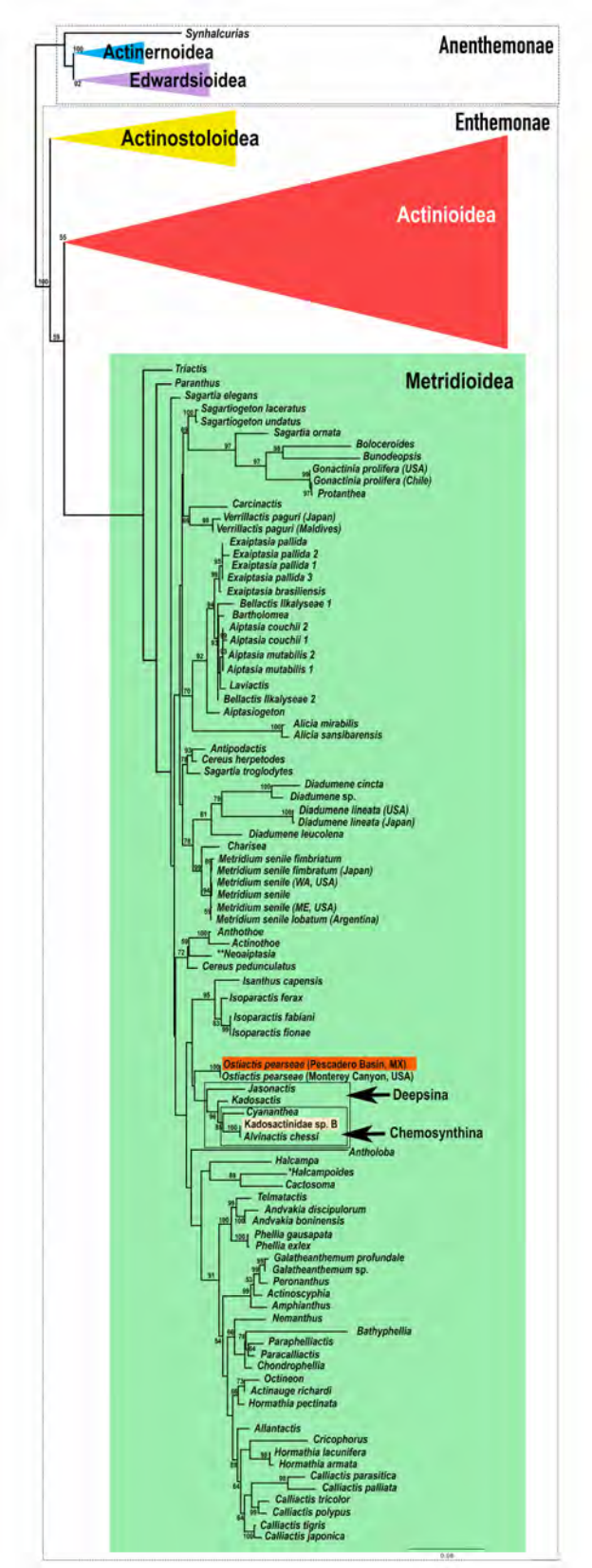
Anenthemonae
Synhalcurias
Actinernoidea
Edwardsioidea
Enthemonae
Actinostoloidea
Actinioidea
Metridioidea
Triactis
Paranthus
Sagartia elegans
Sagartiogeton laceratus
Sagartiogeton undatus
Sagartia ornata
Boloceroides
Bunodeopsis
Gonactinia prolifera (USA)
Gonactinia prolifera (Chile)
Protanthea
Carcinactis
Verrillactis paguri (Japan)
Verrillactis paguri (Maldives)
Exaiptasia pallida
Exaiptasia pallida 2
Exaiptasia pallida 1
Exaiptasia pallida 3
Exaiptasia brasiliensis
Bellactis ilkalyseae 1
Bartholomea
Aiptasia couchii 2
Aiptasia couchii 1
Aiptasia mutabilis 2
Aiptasia mutabilis 1
Laviactis
Bellactis ilkalyseae 2
Aiptasiogeton
Alicia mirabilis
Alicia sansibarensis
Antipodactis
Cereus herpetodes
Sagartia troglodytes
Diadumene cincta
Diadumene sp.
Diadumene lineata (USA)
Diadumene lineata (Japan)
Diadumene leucolena
Charisea
Metridium senile fimbriatum
Metridium senile fimbratum (Japan)
Metridium senile (WA, USA)
Metridium senile
Metridium senile (ME, USA)
Metridium senile lobatum (Argentina)
Anthothoe
Actinothoe
**Neoaiptasia
Cereus pedunculatus
Isanthus capensis
Isoparactis ferax
Isoparactis fabiani
Isoparactis fionae
Ostiactis pearseae (Pescadero Basin, MX)
Ostiactis pearseae (Monterey Canyon, USA)
Jasonactis
Kadosactis
Cyananthea
Kadosactinidae sp. B
Alvinactis chessi
Deepsina
Chemosynthina
Antholoba
Halcampa
*Halcampoides
Cactosoma
Telmatactis
Andvakia discipulorum
Andvakia boninensis
Phellia gausapata
Phellia exlex
Galatheanthemum profundale
Galatheanthemum sp.
Peronanthus
Actinoscyphia
Amphianthus
Nemanthus
Bathyphellia
Paraphelliactis
Paracalliactis
Chondrophellia
Octineon
Actinauge richardi
Hormathia pectinata
Allantactis
Cricophorus
Hormathia lacunifera
Hormathia armata
Calliactis parasitica
Calliactis palliata
Calliactis tricolor
Calliactis polypus
Calliactis tigris
Calliactis japonica
0.09

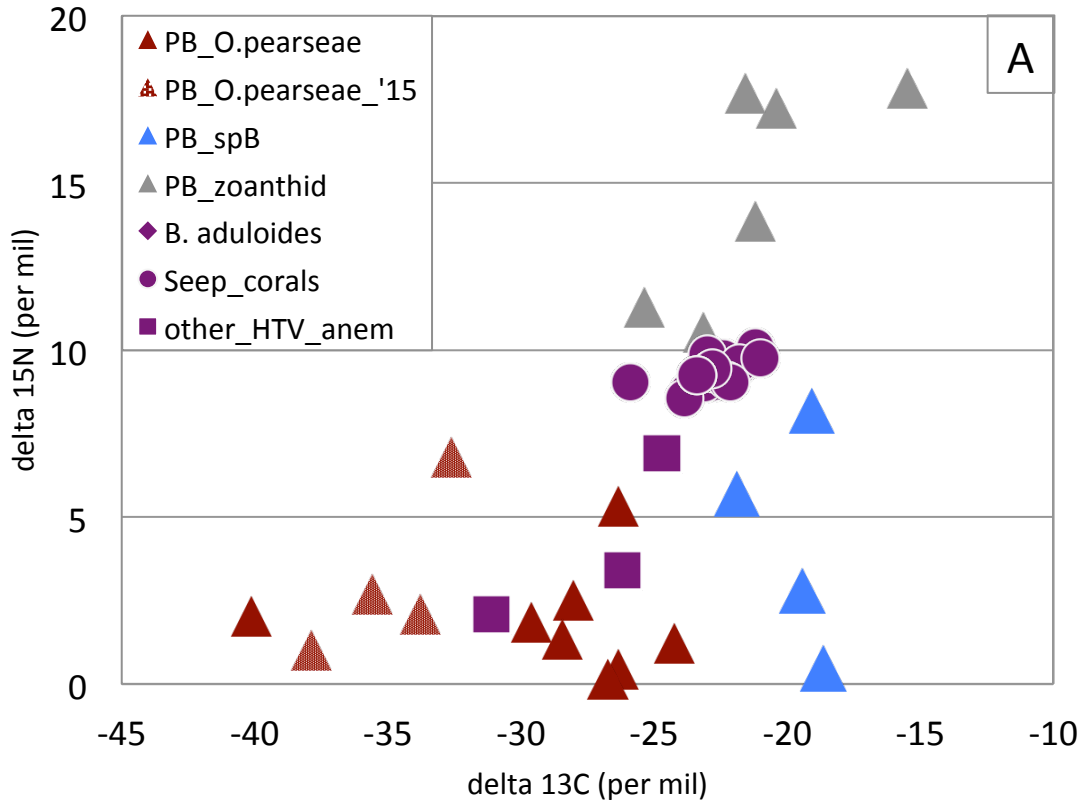

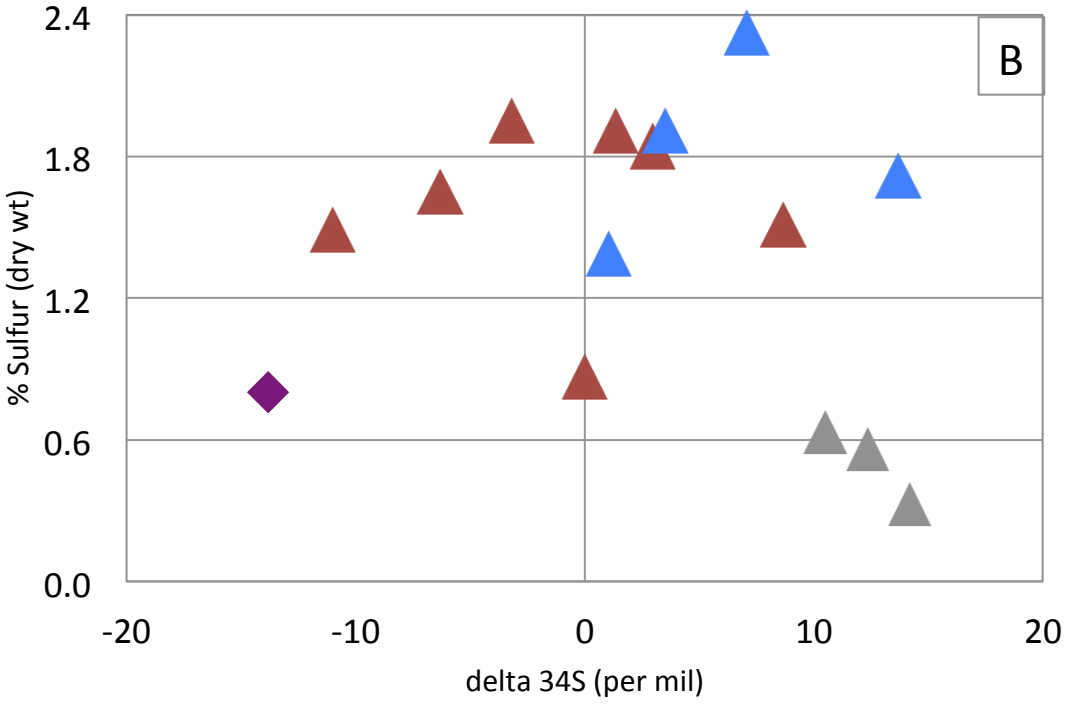

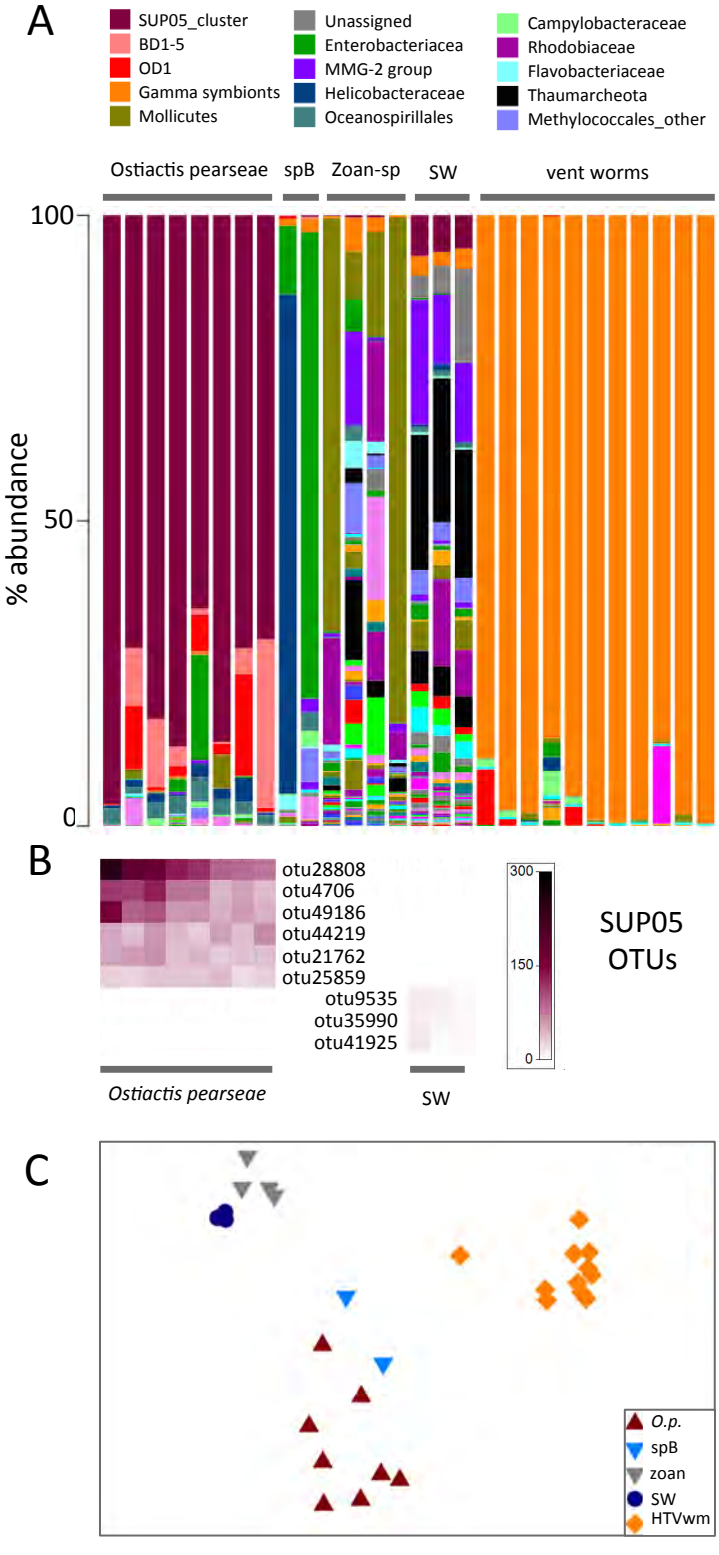
A
SUP05_cluster
BD1-5
OD1
Gamma symbionts
Mollicutes
Unassigned
Enterobacteriacea
MMG-2 group
Helicobacteraceae
Oceanospirillales
Campylobacteraceae
Rhodobiaceae
Flavobacteriaceae
Thaumarcheota
Methylococcales_other
Ostiactis pearseae
spB
Zoan-sp
SW
vent worms
100
50
0
% abundance
B
otu28808
otu4706
otu49186
otu44219
otu21762
otu25859
otu9535
otu35990
otu41925
300
150
0
SUP05 OTUs
Ostiactis pearseae
SW
C
O.p.
spB
zoan
SW
HTVwm

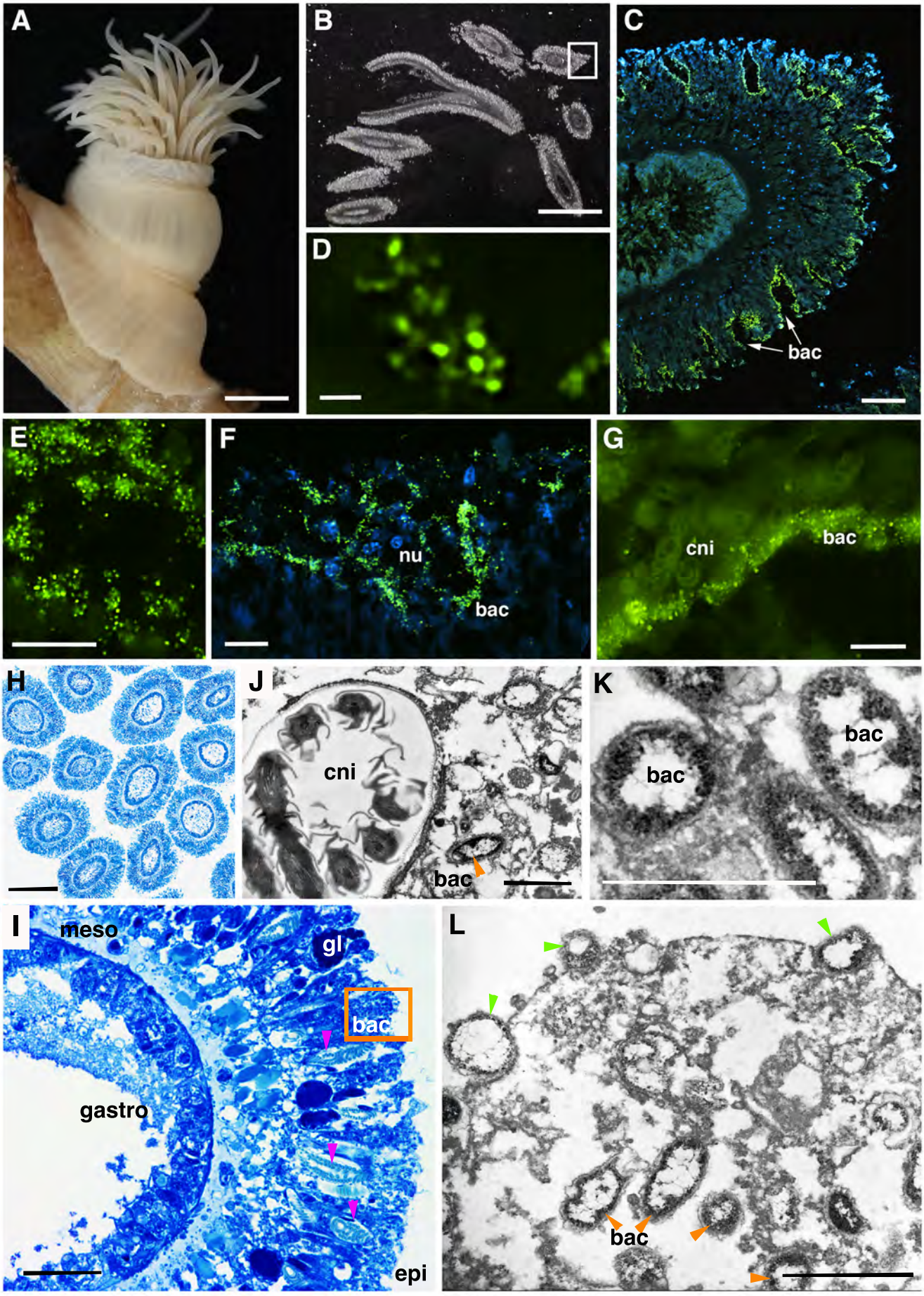

Supplemental Information – Goffredi et al.

Table S1: Number of total 16S rRNA amplicon reads, the Shannon Diversity index (H') and the relative abundance (%) of the SUP05 group (based on 16S rRNA barcode amplification) associated with *Ostiactis pearseae*, water samples, and other Anthozoa from the Pescadero Basin vents.

Table S2: Taxa included in this study, with voucher location and GenBank accession numbers. Taxa are organized alphabetically within their family; new sequences indicated in bold.

Fig. S1 Phylogenetic relationships of the SUP05 group, based on 16S rRNA.
A. SUP05 cluster, based on 16S rRNA. Taxa shown in green are known symbionts of marine invertebrates. * > 70% support (using the Jukes Kantor model). Additional taxa were included according to Petersen et al. 2012; Glaubitz et al. 2013; Shah et al 2019. **Inset**. Shows SUP05 amplicons recovered from *Ostiactis pearseae*, surrounding seawater samples, and *Bathymodiolus* mussels from the Costa Rica margin Jaco Scar seep sites (SG, unpublished).

Fig. S2 Fluorescence Microscopy of the tentacles of *Ostiactis pearseae.*
Fluorescent *in situ* signal amplification via hybridization chain reaction-FISH (HCR-FISH) microscopy of *Ostiactis pearseae* tentacles using **A.** a general bacterial probe set Eub338 I-III, **B.** the specific Anem_SUP05 probe, and **C.** an overlay of the two showing near complete overlap. Scale is 10 μm.

Available from the Dryad Digital Repository (https://doi.org/10.5061/dryad.mkkwh70wt)

Supp Video: Sea anemones were collected by ROV manipulator or suction sampler mounted on ROV *SuBastian*.

DataFile S1
The raw Illumina barcode sequence data and QIIME processed data, including representative sequences for all OTUs, as well as representative sequences for the SUP05 OTUs specifically.

Supp Table 1: Number of total 16S rRNA amplicon reads, the Shannon Diversity index (H') and the relative abundance (%) of the SUP05 group (based on 16S rRNA barcode amplification) associated with *Ostiactis pearseae*, water samples, and other Anthozoa from the Pescadero Basin vents.

Ostiactis pearseae				
Auka vent field	**Dive #-Sample #**	**# of reads**	**H′ index[1]**	**% SUP05**
Matterhorn	S0193-R2	11596	2.13	96.4
E. of Diane's vent	S0193-A2	1852	2.79	70.9
Z vent (top)	S0194-S2	2405	2.60	82.5
S. of Z vent (small chimney)	S0200-R2w	21299	2.67	87.0
JaichMaa 'ja'ag vent field				
Abuelita	S0197	16566	2.90	64.4
Abuelita	S0197-CM2	4356	2.75	86.2
Abuelita	S0197-CM3	6028	2.97	70.9
Weey 'kual	S0199-S8	10220	2.61	69.4
Water Samples				
Auka vent field	**Dive #-Sample #**	**# of reads**	**H′ index[2]**	**% SUP05**
E. of Diane's vent	S0193-N2	15754	4.38	6.7
JaichMaa 'ja'ag vent field				
Abuelita	S0197-N2	24802	4.91	6.0
Weey 'kual	S0199-N1	10457	4.77	5.5
Other Anthozoa				
Auka vent field	**Dive #-Sample #**	**# of reads**	**H′ index[2]**	**% SUP05**
Matterhorn	S0193-S4	1377	2.87	0.0
S. of Z vent (small chimney)	S0200-R2r	2805	3.14	0.3
E. of Diane's vent	S0193-R3	40902	2.82	0.1
Z vent (lower on structure)	S0194-R1	2858	3.64	0.4
NW. of Z vent (diffuse flow)	S0194-R2	2759	3.19	0.3
NW. of Z vent (diffuse flow)	S0194-S1	47970	2.46	0.0

[1] based on OTUs, defined as 99% similar based on 16S rRNA

Table S2								
Higher taxon	Family	Voucher	Genus	Species	12S rRNA	16S rRNA	18S rRNA	COIII
Actinernoidea	Actinernidae	AMNH	*Actinernus*	*antarcticus*	KJ482930	KJ482966	KJ483023	----------
		AMNH	*Isactinernus*	*quadrilobatus*	KJ482932	KJ482968	KJ483024	KJ482998
		NA	*Synhalcurias*	*elegans*	KJ482942	----------	KJ483021	----------
	Halcuriidae	AMNH	*Halcurias*	*pilatus*	KJ482931	KJ482967	KJ483020	KJ482997
Edwardsioidea	Edwardsiidae	AMNH	*Edwardsia*	*elegans*	EU190726	EU190770	EU190857	GU473338
		KUNHM	*Edwardsia*	*japonica*	GU473274	GU473288	GU473304	GU473359
		KBPGI	*Edwardisella*	*loveni*	KX946216	KX946212	KX946218	KX946217
		KUNHM	*Edwardsia*	*timida*	GU473281	KT852113	GU473315	KT852332
		AMNH	*Edwardsianthus*	*gilbertensis*	EU190728	EU190772	EU190859	----------
		KUNHM	*Nematostella*	*vectensis*	EU190750	AY169370	AF254382	FJ489501
Actinioidea	Actiniidae	CAS	*Actinia*	*fragacea*	EU190714	EU190756	EU190845	GU473334
		KUNHM	*Actinia*	*tenebrosa*	KT852045	KT852111	KT852174	KT852330
		KUNHM	*Anemonia*	*erythraea*	KY789302	KY789335	----------	KY789271
		CAS	*Anemonia*	*viridis*	EU190718	EU190760	EU190849	GU473335
		KUNHM	*Anthopleura*	*anneae*	KY789327	KY789360	----------	KY789293
		NA	*Anthopleura*	*artemisia*	KT852015	KT852081	KT852148	KT852300
		NA	*Anthopleura*	*atodai*	KT851993	KT852055	KT852123	KT852275
		KUNHM	*Anthopleura*	*ballii*	KY789311	KY789346	----------	KY789281
		KUNHM	*Anthopleura*	*biscayensis*	KY789315	KY789350	----------	KY789284
		KUNHM	*Anthopleura*	*buddemeieri*	KY789316	KY789351	----------	----------
		KUNHM	*Anthopleura*	*dixoniana*	KY789307	KY789341	----------	KY789276
		KUNHM	*Anthopleura*	*dowii*	KY789318	KY789353	----------	KY789286
		NA	*Anthopleura*	*elegantissima*	EU190713	EU190755	EU190844	GU473333
		KUNHM	*Anthopleura*	*fuscoviridis*	KY789303	KY789336	----------	KY789272
		NA	*Anthopleura*	*handi*	KT852013	KT852079	KT852146	KT852298
		KUNHM	*Anthopleura*	*insignis*	KY789331	KY789364	----------	KY789297
		KUNHM	*Anthopleura*	*krebsi*	KY789305	KY789339	----------	KY789275
		KUNHM	*Anthopleura*	*kurogane* (Korea)	KY789321	KY789355	----------	KY789288
		KUNHM	*Anthopleura*	*midori*	KY789324	----------	----------	KY789289
		KUNHM	*Anthopleura*	*nigrescens* (Galapagos)	----------	KY789343	----------	KY789278
		KUNHM	*Anthopleura*	*pacifica*	KY789309	KY789344	----------	KY789279
		NA	*Anthopleura*	*rosea*	KT852039	KT852104	KT852168	KT852324
		KUNHM	*Anthopleura*	sp. "inornata"	KY789304	KY789338	----------	KY789274
		KUNHM	*Anthopleura*	*thallia*	KY789333	KY789366	----------	KY789300
		KUNHM	*Anthopleura*	*waridi*	KY789301	KY789334	----------	KY789270
		KUNHM	*Anthostella*	*stephensoni*	JQ810719	JQ810721	JQ810723	JQ810726
		NA	*Aulactinia*	*incubans*	KT852014	KT852080	KT852147	KT852299
		AMNH	*Aulactinia*	*marplatensis*	KT851999	KT852061	KT852129	KT852281
		AMNH	*Aulactinia*	*stella*	KT852044	KT852110	KT852173	KT852329
		AMNH	*Aulactinia*	*vancouverensis*	KT852019	KT852085	KT852151	KT852305
		AMNH	*Aulactinia*	*veratra*	KT852001	KT852063	KT852131	KT852283
		AMNH	*Bolocera*	*kerguelensis*	KJ482925	KJ482965	KJ483029	KJ482985
		NA	*Bunodactis*	*reynaudi*	KT852041	KT852106	KT852170	KT852326
		KUNHM	*Bunodactis*	*verrucosa*	EU190723	EU190766	EU190854	FJ489484
		KUNHM	*Bunodosoma*	*cavernatum*	KY789313	KY789348	----------	KY789282
		KUNHM	*Bunodosoma*	*grandis*	EU190722	EU190765	EU190853	GU473336
		KUNHM	*Bunodosoma*	*granuliferum*	KY789314	KY789349	----------	KY789283
		MV	*Epiactis*	*australiensis*	KT852000	KT852062	KT852130	KT852282
		NA	*Epiactis*	*fernaldi*	KT852005	KT852068	KT852136	KT852288
		NA	*Epiactis*	*georgiana*	KT852007	KT852070	KT852138	KT852290
		AMNH	*Epiactis*	*handi1*	KT851988	KT852050	KT852118	KT852269
		AMNH	*Epiactis*	*handi2*	KT851990	KT852052	KT852120	KT852271
		AMNH	*Epiactis*	*japonica1*	KT851991	KT852053	KT852121	KT852272
		AMNH	*Epiactis*	*japonica2*	KT852048	KT852116	KT852178	KT852333
		AMNH	*Epiactis*	*japonica3*	KY789317	KY789352	----------	KY789285
		AMNH	*Epiactis*	*lisbethae1*	KT852006	KT852069	KT852137	KT852289
		AMNH	*Epiactis*	*lisbethae2*	EU190727	EU190771	EU190858	GU473360
		AMNH	*Epiactis*	*prolifera*	KT851989	KT852051	KT852119	KT852270
		AMNH	*Epiactis*	*ritteri1*	KT851994	KT852056	KT852124	KT852276
		AMNH	*Epiactis*	*ritteri2*	KT851995	KT852057	KT852125	KT852277
		AMNH	*Epiactis*	*thompsoni*	KT852011	KT852074	KT852142	KT852294
		AMNH	*Glyphoperidium*	*bursa*	KJ482923	KJ482961	KJ483033	KJ482982
		NA	*Gyractis*	*sesere*	KT852012	KT852078	KT852145	KT852297
		AMNH	*Isactinia*	*olivacea*	----------	KT852077	KT852144	KT852296
		AMNH	*Isotealia*	*antarctica*	JQ810720	JQ810722	----------	JQ810727
		AMNH	*Korsaranthus*	*natalensis*	KJ482920	KJ482958	KJ483017	KJ482987
		KUNHM	*Macrodactyla*	*doreenensis*	EU190739	EU190785	EU190867	GU473342
		AMNH	*Oulactis*	*muscosa*	KT852033	KT852097	KT852162	KT852317
		KUNHM	*Phlyctenactis*	*tuberculosa*	KY789326	KY789359	----------	KY789292
		KUNHM	*Pseudactinia*	*varia*	KY789328	KY789361	----------	KY789294
		KUNHM	*Urticina*	*coriacea*	GU473282	EU190797	KT852176	GU473351
		AMNH	*Urticina*	*crassicornis*	KT851997	KT852059	KT852127	KT852279
		CMNI	*Urticina*	*fecunda*	KT852004	KT852067	KT852135	KT852287
		AMNH	*Urticina*	*grebelnyli*	KT852034	KT852098	KT852163	KT852318
	Actinodendridae	KUNHM	*Actinostephanus*	*haeckeli*	KJ482936	EU190762	KJ483034	GU473353
	Capneidae	AMNH	*Capnea*	*georgiana*	----------	KJ482951	KJ483022	KJ482990

	Condylanthidae	AMNH	*Charisea*	*saxicola*	KT852020	KT852086	KT852152	KT852306
	Haloclavidae	KUNHM	*Haloclava*	sp.	KJ482924	KJ482963	KJ483031	KJ482989
		AMNH	*Haloclava*	*producta*	EU190734	EU190779	AF254370	JF833008
		AMNH	*Harenactis*	*argentina*	KJ482926	KJ482964	KJ483026	KJ482984
		KUNHM	*Peachia*	*cylindrica*	EU190743	EU190789	KJ483015	----------
		AMNH	*Stephanthus*	*antarcticus*	KJ482927	KJ482960	KJ483019	KJ482983
	Liponematidae	KUNHM	*Liponema*	*brevicornis*	EU190738	EU190784	EU190866	KJ483001
		AMNH	*Liponema*	*multiporum*	KJ482922	KJ482962	----------	----------
	Phymanthidae	KUNHM	*Phymanthus*	*loligo*	EU190745	EU190791	EU190871	GU473345
		AMNH	*Phymanthus*	*crucifer1*	KJ910343	KJ910345	MH670399	KJ910346
		AMNH	*Phymanthus*	*crucifer2*	KJ910344	KJ910345	MH670402	KJ910346
		AMNH	*Phymanthus*	*crucifer3*	KJ910343	KJ910345	MH670404	KJ910346
	Preactiidae	AMNH	*Preactis*	*milliardae*	KJ482921	KJ482957	KJ483018	KJ482986
		AMNH	*Dactylanthus*	*antarcticus*	GU473272	AY345877	AF052896	GU473358
	Stichodactylidae	KUNHM	*Heteractis*	*magnifica*	EU190732	EU190777	EU190862	KJ482988
		KUNHM	*Stichodactyla*	*gigantea*	EU190747	EU190793	----------	KY789299
Actinostoloidea	Actinostolidae	AMNH	*Actinostola*	*chilensis*	----------	GU473285	GU473302	GU473357
		AMNH	*Actinostola*	*crassicornis*	----------	EU190753	EU190843	GU473332
		AMNH	*Actinostola*	*georgiana*	KJ482928	KJ482952	KJ483032	KJ482991
		AMNH	*Antholoba*	*achates**	GU473269	GU473284	GU473301	GU473356
		AMNH	*Anthosactis*	*janmayeni*	KJ482938	GU473292	GU473308	GU473363
		AMNH	*Hormosoma*	*scotti*	EU190733	EU190778	EU190863	GU473366
		AMNH	*Paranthus*	*niveus**	GU473277	GU473295	GU473311	GU473344
		KUNHM	*Stomphia*	*didemon*	KJ482929	EU190795	EU190875	GU473348
		AMNH	*Stomphia*	*selaginella*	GU473280	GU473298	GU473314	GU473349
Metridioidea	Actinoscyphiidae	AMNH	*Actinoscyphia*	*plebeia*	EU190712	EU190754	FJ489437	FJ489476
	Aiptasiidae	AMNH	*Aiptasia*	*couchii1*	KP761199	KP761254	KP761301	KP761405
		AMNH	*Aiptasia*	*couchii2*	KP761200	KP761255	KP761303	KP761403
		KUNHM	*Aiptasia*	*mutabilis1*	JF832963	FJ489418	FJ489438	FJ489505
		AMNH	*Aiptasia*	*mutabilis2*	KP761194	KP761248	KP761300	KP761404
		AMNH	*Aiptasiogeton*	*hyalinus*	KR704266	KR186040	KR704268	----------
		AMNH	*Bartholomea*	*annulata*	EU190721	EU190763	EU190851	FJ489483
		AMNH	*Bellactis*	*ilkalyseae1*	----------	KP761238	KP761316	KP761393
		AMNH	*Bellactis*	*ilkalyseae2*	KR186020	KR186036	KR186051	----------
		AMNH	*Exaiptasia*	*brasiliensis*	KP761188	KP761239	KP761312	KP761386
		AMNH	*Exaiptasia*	*pallida1*	KP761183	KP761270	KP761286	----------
		AMNH	*Exaiptasia*	*pallida2*	KP761176	KP761226	KP761280	KP761376
		AMNH	*Exaiptasia*	*pallida3*	KP761177	KP761227	KP761322	KP761377
		AMNH	*Laviactis*	*lucida*	KP761192	KP761243	KP761296	KP761402
		KUNHM	*Neoaiptasia*	*morbilla***	EU190742	EU190788	----------	JF833010
	Aliciidae	AMNH	*Alicia*	*mirabilis*	KP761213	----------	KP761310	KP761410
		AMNH	*Alicia*	*sansibarensis*	KJ482933	KJ482953	KJ483016	KJ483000
		KUNHM	*Triactis*	*producta*	EU490525	----------	EU190876	GU473350
	Amphianthidae	USNM	*Amphianthus*	sp.	FJ489413	FJ489432	FJ489450	FJ489502
		AMNH	*Peronanthus*	sp.	KJ482917	KJ482956	KJ483014	KJ482976
	Andvakiidae	KUNHM	*Andvakia*	*boninensis*	EU190717	EU190759	EU190848	FJ489479
		KUNHM	*Andvakia*	*discipulorum*	GU473273	GU473287	GU473316	----------
		AMNH	*Telmatactis*	sp.	JF832968	JF832979	KJ483013	----------
	Antipodactinidae	AMNH	*Antipodactis*	*awii*	GU473271	GU473286	GU473303	GU473337
	Bathyphelliidae	KUNHM	*Bathyphellia*	*australis*	FJ489402	FJ489422	EF589063	FJ489482
	Boloceroididae	KUNHM	*Boloceroides*	*mcmurrichi*	GU473270	----------	EU190852	----------
		AMNH	*Bunodeopsis*	*globulifera*	KJ482940	KJ482949	KJ483025	KJ482992
	Diadumenidae	KUNHM	*Diadumene*	*cincta*	EU190725	EU190769	EU190856	FJ489490
		KUNHM	*Diadumene*	*leucolena*	JF832957	JF832977	JF832986	JF833006
		KUNHM	*Diadumene*	sp.	JF832960	JF832976	JF832980	JF833005
		KUNHM	*Diadumene*	*lineata* (Japan)	JF832965	JF832973	JF832987	JF833007
		KUNHM	*Diadumene*	*lineata* (USA)	EU190730	EU190774	EU190860	FJ489506
	Galatheanthemidae	AMNH	*Galatheanthemum*	*profundale*	KJ482919	KJ482954	KJ483011	KJ482978
		AMNH	*Galatheanthemum*	sp. nov.	KJ482918	KJ482955	KJ483012	KJ482977
	Gonactiniidae	AMNH	*Gonactinia*	*prolifera* (Chile)	KJ482935	----------	KJ483008	KJ482994
		AMNH	*Gonactinia*	*prolifera* (USA)	KJ482937	KJ482969	KJ483009	KJ482995
		AMNH	*Protantea*	*simplex*	KJ482939	KJ482970	KJ483010	KJ482993
	Halcampidae	AMNH	*Cactosoma*	sp. nov.	FJ489407	GU473297	GU473313	GU473346
		KUNHM	*Halcampa*	*duodecimcirrata*	JF832966	EU190776	AF254375	----------
		AMNH	*Halcampoides*	*purpureus*	EU190735	EU190780	AF254380	----------
	Hormathiidae	KUNHM	*Actinauge*	*richardi*	EU190719	EU190761	EU190850	FJ489480
		KUNHM	*Allantactis*	*parasitica*	FJ489399	FJ489420	FJ489439	FJ489478
		KUNHM	*Calliactis*	*japonica*	FJ489403	FJ489423	FJ489441	FJ489486
		KUNHM	*Calliactis*	*palliata*	FJ489398	FJ489419	FJ489436	FJ489474
		KUNHM	*Calliactis*	*parasitica*	EU190711	EU190752	EU190842	FJ489475
		KUNHM	*Calliactis*	*polypus* (Hawaii)	FJ489407	FJ489427	FJ489445	FJ489485
		KUNHM	*Calliactis*	*tricolor*	FJ489405	FJ489425	FJ489443	FJ489488
		AM	*Calliactis*	*tigris*	MK801512	MK801514	MK801510	MK801561
		USNM	*Chondrophellia*	*orangina*	FJ489406	FJ489426	FJ489444	FJ489489
		AMNH	*Cricophorus*	*nutrix*	----------	KT852066	KT852134	KT852286
		AMNH	*Hormathia*	*armata*	EU190731	EU190775	EU190861	FJ489491
		AMNH	*Hormathia*	*lacunifera*	FJ489409	FJ489428	FJ489446	FJ489492

		AMNH	*Hormathia*	*pectinata*	FJ489415	FJ489430	FJ489448	FJ489497
		CMHN	*Paracalliactis*	*japonica*	FJ489411	FJ489429	FJ489447	FJ489496
		AMNH	*Paracalliactis*	sp.	MK801513	MK801515	MK801511	MK801562
		KUNHM	*Paraphelliactis*	sp.	FJ489412	FJ489431	FJ489449	FJ489498
	Isanthidae	AMNH	*Isanthus*	*capensis*	JF832967	GU473291	GU473291	GU473362
		AMNH	*Isoparactis*	*fabiani*	JF832964	GU473283	GU473300	GU473355
		AMNH	*Isoparactis*	*fionae*	KC700001	KC700003	KC700004	KC700007
		AMNH	*Isoparactis*	*ferax*	KC700002	----------	KC700005	KC700008
	Kadosactinidae	USNM	*Alvinactis*	*chessi*	GU473278	GU473296	GU473312	GU473352
		NA	**Kadosactinidae**	**sp.**	**TBD**	**TBD**	----------	**TBD**
		USMN	*Cyananthea*	*hourdezi*	GU473275	GU473293	GU473309	GU473364
		USNM	*Jasonactis*	*erythraios*	----------	GU473289	GU473305	GU473339
		AMNH	*Kadosactis*	*antarctica*	FJ489410	EU190782	EU190865	FJ489504
	Metridiidae	KUNHM	*Metridium*	*senile fimbriatum*	KT852023	KT852089	JF832988.1	KT852309
		KUNHM	*Metridium*	*s. fibratum* (Japan)	----------	JF832974	JF832988	JF833009
		KUNHM	*Metridium*	*s. lobatum* (Argentina)	JF832962	JF832971	JF832981	JF833002
		KUNHM	*Metridium*	*senile*	KT852024	EU190786	AF052889	FJ489494
		AMNH	*Metridium*	*senile* (ME, USA)	KJ482916	KJ482950	KJ483035	KJ482975
		KUNHM	*Metridium*	*senile* (WA, USA)	EU190740	JF832972	JF832982	JF833003
	Nemanthidae	KUNHM	*Nemanthus*	*nitidus*	EU190741	EU190787	EU190868	FJ489495
	Ostiactinidae	CAS	*Ostiactis*	*pearseae* (Monterey Ca	EU190751	EU190798	EU190878	GU473365
		SIO	***Ostiactis***	***pearseae* (Pescadero B**	**TBD**	**TBD**	**TBD**	**TBD**
	Phellidae	ZSM	*Phellia*	*exlex*	JF832958	JF832978	JF832984	JF833004
		KUNHM	*Phellia*	*gausapata*	EU190744	EU190790	EU190870	FJ489473
	Sagartiidae	ZSM	*Actinothoe*	*sphyrodeta*	FJ489401	FJ489421	FJ489440	FJ489481
		ZSM	*Anthothoe*	*chilensis*	FJ489397	FJ489416	FJ489434	FJ489470
		KUNHM	*Cereus*	*herpetodes*	JF832956	JF832969	JF832983	----------
		KUNHM	*Cereus*	*pedunculatus*	EU190724	EU190767	EU190855	FJ489471
		KUNHM	*Sagartia*	*elegans*	----------	JF832970	JF832989	JF833012
		AMNH	*Sagartia*	*ornata*	JF832959	JF832975	JF832985	JF833011
		KUNHM	*Sagartia*	*troglodytes*	EU190746	KT852107	EU190872	FJ489499
		KUNHM	*Sagartiogeton*	*laceratus*	EU190748	EU190794	EU190874	FJ489500
		KUNHM	*Sagartiogeton*	*undatus*	FJ489400	FJ489417	FJ489435	FJ489472
		KUNHM	*Verrillactis*	*paguri*	FJ489414	FJ489433	FJ489440	FJ489503

* Although these species fall within superfamily Metridioidea in most recent phylogenetic studies (see Rodríguez et al. 2014), we follow the classification of Carlgren (1949) until further revision; ** this species is not an Aiptasiidae (see Grajales and Rodríguez 2016) but its taxonomic position is unclear, we follow the classification of Carlgren (1949) until further revision. AM: Australian Museum; AMNH: American Museum of Natural History; CAS: California Academy of Sciences; FMNH: Field Museum of Natural History; KUNHM: University of Kansas Natural History Museum; MNHG: Museum of Natural History of Geneva; RMNH: Rijksmuseum van Natuurlijke Historie; SOI: Scripps Oceanic Institution; USNM: U. S. National Museum of Natural History; ZSM: Bavarian State Collection of Zoology; NA: voucher not available.

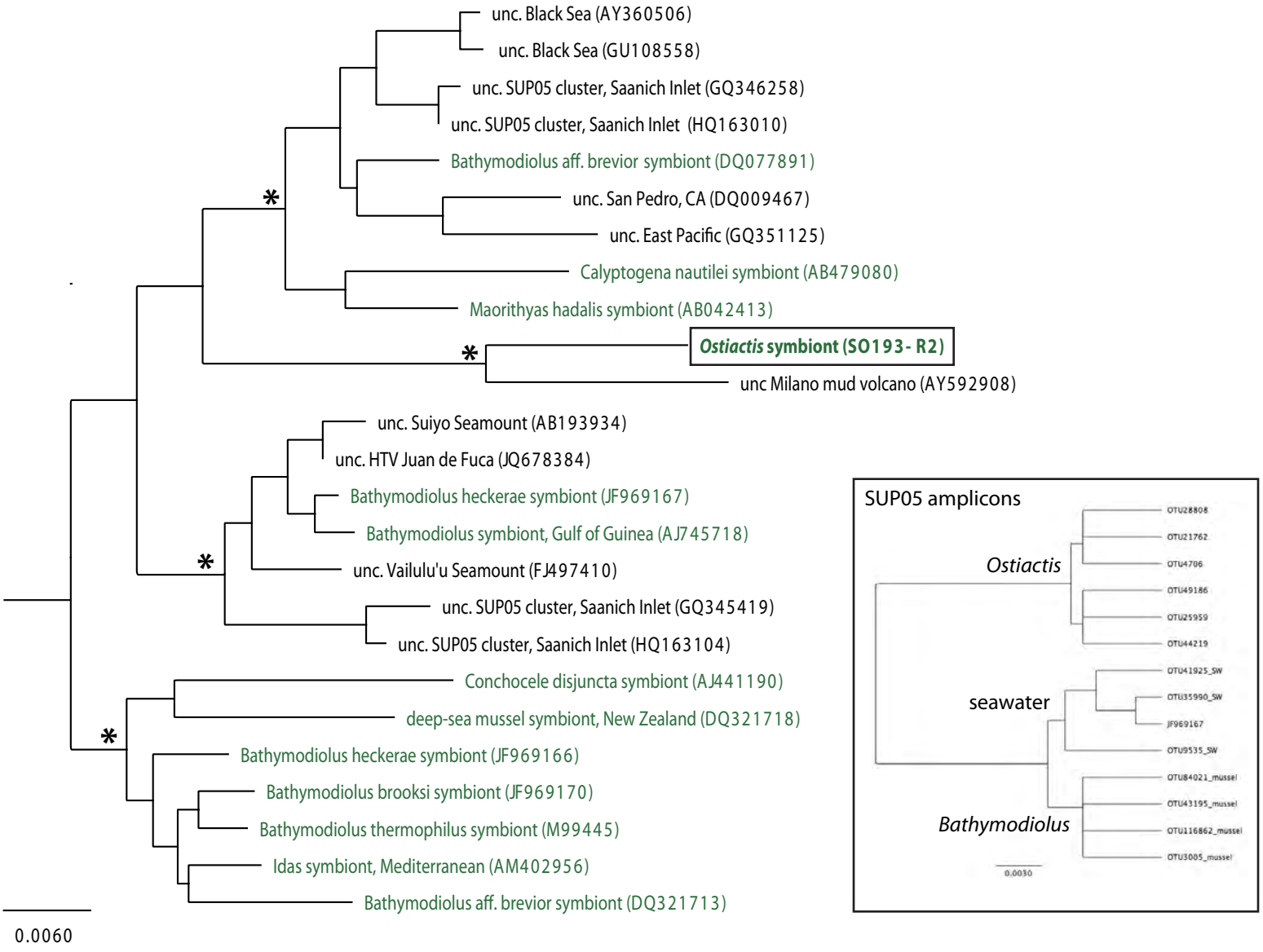

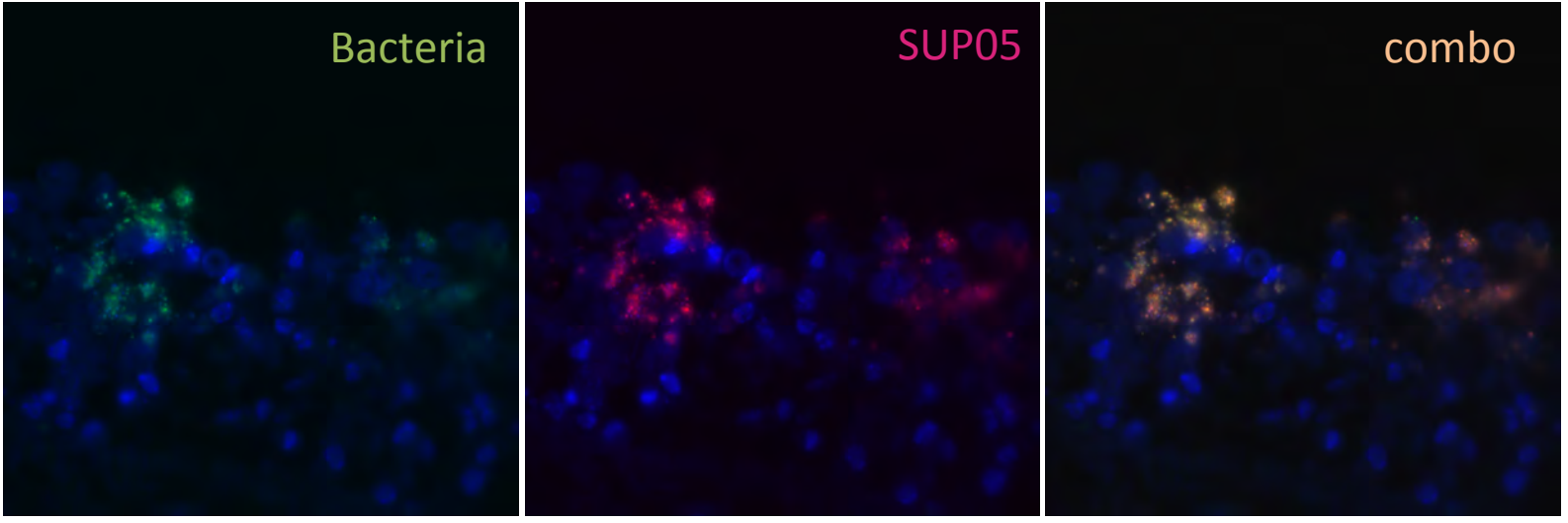
Bacteria
SUP05
combo